Utrecht University

The effect of shoreward propagating accretionary waves on the intertidal beach

MSc Thesis

Dennis Korevaar

The effect of shoreward propagating accretionary waves on the intertidal beach

MSc Thesis

Final version

Korevaar, D. (Dennis)

4151992

Earth Surface and Water

31/05/2018

Supervisors:

Dr. T.D. Price

Prof. Dr. B.G. Ruessink

Utrecht University

Faculty of Geosciences

Department of Physical Geography

Abstract

The horn of a bar can separate and migrate onshore as an individual coherent feature. These features are named Shoreward Propagating Accretionary Waves (SPAWs). To better understand SPAWs, the effect of these features on the intertidal beach was determined for the Egmond coast by making use of Argus imagery. For all selected days the shoreline was mapped for all Argus images available on that day with the Intertidal Beach Mapper (IBM). With a loess interpolation a bathymetry was determined from these shorelines. In addition, barlines which were classified for each day of the study period with the BarLine Intesity Mapper (BLIM) were used. From these data the width, volume, alongshore variability and morphology of the intertidal area were determined. After the SPAW emerged from the inner bar the alongshore variability of the shoreline increased. A seaward protrusion was already present shoreward of the SPAW. Until the period the SPAW welded to the beach the seaward protrusion grew and the volume of the intertidal beach increased with ~4000 m^3. When the SPAW welded to the beach the volume of the intertidal area increased with ~6000 m^3 in just two weeks, which corresponds to an onshore sediment flux of ~2.0 m^3/m/day, and the shoreline moved even more seaward. In the following period the sediment was transported in alongshore and cross-shore direction. The alongshore variability decreased from ~30 m to ~15 m for the low tide line in just two months because the sand dispersed alongshore, forming a new intertidal bar. The mean location of the high tide line moved seaward and its alongshore variability increased. Sediment from the lower intertidal area was transported to the upper intertidal area to even further shoreward because of the increase in intertidal beach width. Because there was a large data gap the exact period the intertidal beach was affected by the SPAW event is unknown, but it could be said that it ranged between 2 and 6 months.

Keywords: morphodynamics, SPAW, video imaging, IBM, intertidal beach, alongshore variability

Table of Contents

Chapter 1 Introduction

The beach is the connection between the nearshore and the dunes. During storm conditions the beach-dune system is eroded and sand is transported from the beach and dune system to the nearshore by wave-induced processes while during calm conditions the sand is transported back on the beach by wave action. When deposited on the beach wind-induced sediment transport will return the sand to the dune system again. Where the erosion of the beach-dune system is a fast process which can happen in one storm event, the recovery of the beach-dune system can take months to years. Alongshore variations in the morphology of the beach can also result in striking alongshore variability in beach-dune erosion (Thornton et al., 2007; Castelle et al., 2015). This alongshore variability in morphology of the beach affects the also alongshore variable recovery of the dune system. Sandy wave-dominated coasts are often characterised by one or more sandbars. In a beach system with multiple sandbars these bars can show coupling (e.g. Bowman and Goldsmith, 1983; Castelle et al., 2007; Price and Ruessink, 2013). The inner bar can also be coupled to the shoreline and therefore affects the alongshore variability and morphology of the beach (e.g., Sonu, 1973; Coco et al. 2005; Thornton et al., 2007; Quartel, 2009; Price and Ruessink, 2013; Van de Lageweg et al., 2013). So, the alongshore variability in subtidal morphology results in the alongshore variability in dune recovery (Keijsers et al., 2014; Castelle et al., 2015).

Nearshore bars are often alongshore variable. This variability is often characterised by landward-protruding shallower areas (horns) and seaward-protruding deeper areas (embayments) at regular intervals (Van Enckevort et al., 2004; Price and Ruessink, 2011). The alongshore variability in wave filtering, which is caused by the difference in water depth alongshore, affects the morphodynamics of the beach. However, there is another process related to the alongshore variability of the nearshore bars which may affect the alongshore variability of the beach. Wijnberg and Holman (2007) and Almar et al. (2010) identified that the horn of a nearshore bar may separate to migrate onshore as an individual coherent feature. These features are known as SPAWs, Shoreward Propagating Accretionary Waves (Wijnberg and Holman, 2007). Only limited research is conducted to understand these SPAWs and therefore the effect on the bar-beach-dune system is still unknown. However, it is known these SPAWs result in a large input of sand to the beach, locally affecting the dimensions of the beach (Wijnberg and Holman, 2007; Almar et al, 2010; Van der Weerd, 2012; De Wit, 2017; Price et al., 2017). The welding of the SPAW to the beach could result in a local increase of the beach width. An increase in beach width affects the magnitude of wind-induced transport and dune development (Aagaard et al., 1998a; Christiansen and Davidson-Arnott, 2004; Thornton et al., 2007; Keijsers et al., 2014). To better determine the development of the coast, it is important to know what the effect of these SPAWs is on the beach-dune system. With this knowledge it could be better determined which parts of the beach are more prone to erosion and should be strengthened, so coastal safety can be guaranteed. A way to strengthen the beach-dune system is the implementation of foreshore nourishments. The research on SPAWs could be used to place the nourishments on locations where the nourishments are more efficient in strengthening the beach-dune system, but also research on SPAWs could give more insight in the dynamics of nourishments because SPAWs can be seen as small natural nourishments (Van der Weerd, 2012).

To better understand the effect of SPAW events on the (intertidal) beach, video images from the ARGUS video tower at Egmond aan Zee were used to determine the development of the dimensions of the intertidal beach. With the Intertidal Beach Mapper (IBM) developed by Aarninkhof et al. (2003)

shorelines will be mapped which were used to determine the intertidal beach width and intertidal beach volume. Also, shorelines collected with the BarLine Intensity Mapper (BLIM) were used.

First, in Chapter 2, a literature overview will be given to better understand the subject. The section starts with an overview of important aspects of the intertidal beach and then focusses on SPAWs. Based on this information the research objective and questions will be introduced. In Chapter 3 the study area and data collection will be described. Then, in Chapter 4, the methodology will be described and its reliability will be evaluated. In Chapter 5 the results of the study will be introduced. The method and results will be discussed in Chapter 6 and finally the main conclusions and recommendations will be stated in Chapter 7.

Chapter 2 Literature review

In this study the focus will be on the impact of Shoreward Propagating Accretionary Waves, abbreviated as SPAWs, on the dimensions of the intertidal beach. Therefore, the relevant processes acting on the intertidal beach/shoreline and the connection of the intertidal beach with the dunes will be discussed in this first section. In the second section the available knowledge on SPAWs will be discussed and in the last section the objective of this study will be made clear.

2.1 The intertidal beach and shoreline

2.1.1 Definition

The beach can be divided in three tide-related zones: the subtidal zone (shoreface), the intertidal zone (foreshore), and the supratidal zone (backbeach). The subtidal zone is the part of the beach that is always submerged by water and the intertidal zone is the part of the beach which is dry during low tide and submerged during high tide. The supratidal zone is the part of the beach above high tide. The width of these zones is determined by the slope of the shoreface and the tidal range. The slope of the shoreface is depended on the sediment size, modal wave height and wave period (Wrigth and Short, 1984). The shoreline is the physical interface between water and land (Dolan et al., 1980). This idealized definition is a challenge to apply because of its temporal and spatial variability.

2.1.2 Wave processes in the intertidal zone

All three morphodynamic zones (the shoaling zone, breaking/surf zone and swash zone) occur in the intertidal area. This means the stage of the tide affects the sediment transport in this region (Masselink and Turner, 1999; Price and Ruessink, 2008) and can therefore be important for the welding of a SPAW to the beach. A combination of swash, surf and shoaling zone processes will be present during a neap-spring tidal cycle in the intertidal zone. The importance of each process will be different in time and space (Wright et al., 1982; Price and Ruessink, 2008). This variability in wave processes can result in different sediment transport rates and directions at one location in the intertidal zone over time (Masselink et al., 2006). At high tide the water level is high thus the waves do not break on the intertidal bar and the surf zone and swash zone are present at the beach. The effect of swash and surf zone processes increases towards the spring high tide level (Masselink, 1993). When the tide drops, the water level decreases and the waves do break on the intertidal bar resulting in a second surf zone around the bar. This occurs earlier in time with high wave conditions because high waves break in larger water depths. When the tide drops even further, one large surf zone is present, because the waves now also break in the trough between the intertidal bar and the beach. This is shown in Figure 2.1 where first the surf zone was present at the beach, then also covered the bar and eventually also covered the area between the bar and the beach. During low wave conditions, the intertidal bar was a barrier for the incoming waves. This resulted in the presence of the surf zone and swash zone on the intertidal bar during low tide. This can be seen in Figure 2.2 where the swash and surf zone migrated offshore over time. During low energy wave conditions, the width of the swash and surf zone was small and their horizontal movement compared to their width was large. During high wave conditions, the horizontal movement compared to the width was relatively small (Price and Ruessink, 2008). During neap tide there is more potential for morphological change than during spring tide. This is caused by the fact that during neap tide the intertidal zone is smaller than during spring tide and certain processes can affect one location longer (Kroon and Masselink, 2002). The morphological change is especially

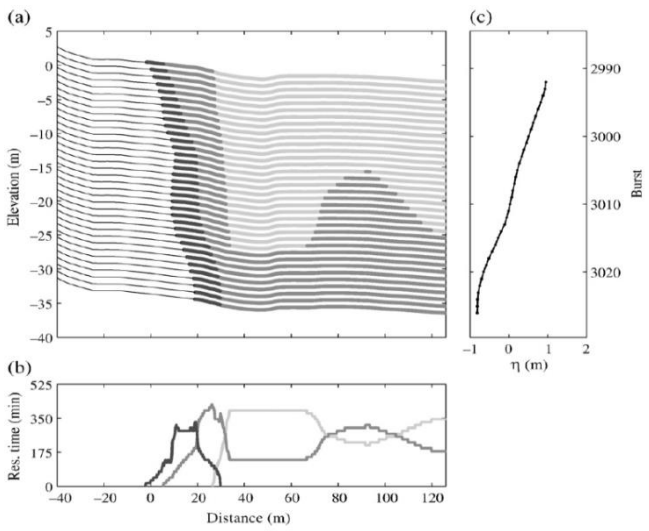

Figure 2.1. (a) Morphodynamic zone distribution and (b) residence time (in minutes) versus cross-shore distance over half a tidal cycle during high-energy conditions. In (a) and (b), the dark grey represents the swash zone, the medium grey the surf zone, and the light grey the shoaling zone. The thin lines in (a) are the subaerial parts of the beach. Note that in (a) each subsequent profile is offset by −1 m. Panel (c) shows the offshore water level η for reference. (Price and Ruessink, 2008).

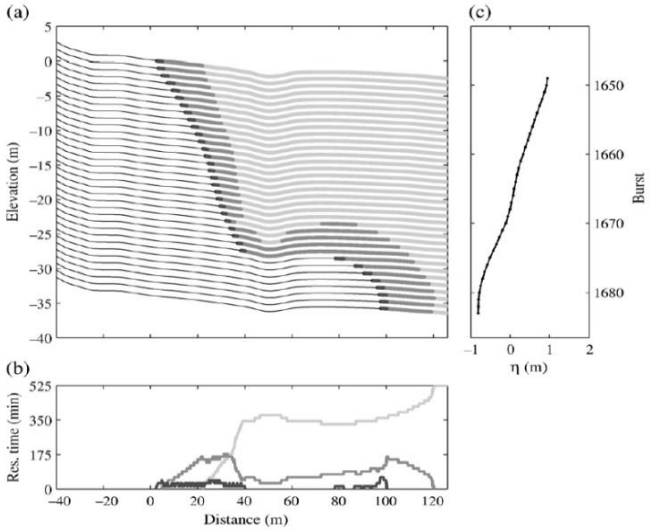

Figure 2.2. (a) Morphodynamic zone distribution and (b) residence time (in minutes) versus cross-shore distance over half a tidal cycle during low-energy conditions. In (a) and (b), the dark grey represents the swash zone, the medium grey the surf zone, and the light grey the shoaling zone. The thin lines in (a) are the subaerial parts of the beach. Note that in (a) each subsequent profile is offset by −1 m. Panel (c) shows the offshore water level η for reference. (Price and Ruessink, 2008).

expected in the lower part of the intertidal zone, because here swash (onshore transport), bores (onshore transport), the bed return flow (offshore transport) and shoaling waves (onshore transport) can be present during one tidal cycle (Masselink et al., 2006).

Price and Ruessink (2008) studied the morphodynamic zone variability at Egmond using the relative tide range (RTR). The relative tide range is the ratio of the tide to the wave height. A RTR larger than 5 resulted in shoaling wave processes across almost the whole intertidal area, with surf zone processes acting on the beach. For a RTR between 2 and 5 the surf zone processes occurred over the intertidal bar and the lower part of the beach face. The swash zone was mainly located on the upper beach face. The surf zone processes around low tide caused the intertidal bar to migrate onshore. This also resulted in steepening of the beach face. For a RTR below 2 the surf zone processes still dominated over the intertidal bar. However, in this case it led to offshore migration of the intertidal bar. The swash zone processes now dominated most of the beach face and resulted in erosion of the upper beach face (Price and Ruessink, 2008).

2.1.3 Intertidal bars

Just like in the subtidal zone the intertidal zone can also have bars. The intertidal bars are locally high morphological features between the low and high water level, and occur on beaches with a significant tidal range (>1 m). Intertidal bars can be intersected by rip channels which drain the trough landward of the bar. The intertidal bar and the intertidal trough are referred to as the intertidal bar system. Multiple intertidal bars can be present ranging from 1 to more than 10. The average dimensions of the intertidal bars are 0.5, 20 and 100 m for height, width and length, respectively (Masselink et al., 2006).

Three intertidal bar types can be distinguished based on their morphology: slip-face bars, low-amplitude ridges and sand waves (Fig. 2.3) (Masselink et al., 2006). A slip-face bar is a bar with a pronounced landward-facing slip face. The difference between the trough landward of the bar

(named runnel) and the intertidal bar crest often varies between tens of centimeters to over a meter and the slope of the slip-face is generally up to the angle of repose (30-35°) (Wijnberg and Kroon, 2002; Masselink et al., 2006). On the other hand, the shoreward-facing slope is very gentle with a slope of 3-6° (Masselink et al., 2006). Slip-face bars generally have an elongated shape and line up more or less with the shoreline (Wijnberg and Kroon, 2002). The spacing of the rip channels which intersect the intertidal bars is very highly variable fluctuating between several tens of meters to a couple hundreds of meters (Short, 1985). The average onshore propagation speed is in the order of 1 m/day (Owens and Frobel, 1977; Kroon, 1994). The bar will migrate onshore as long as the swash overtops the bar crest (Wijnberg and Kroon, 2002). The occurrence of slip-face bars is characterised by a gentle nearshore slope (~ 2°), variable wave conditions and a micro- or mesotidal regime. The formation of slip-face bars is related to storm activity (Davis et al., 1972). During storms beach erosion occurs. As a result, the beach becomes planar or concave. This results in deposition of sediment in the low tide area. In the following days, a ridge is formed. The exact mechanism for the formation of the ridge is not well understood, but it is probably related to swash and backswash processes in combination with the still water level during low tide (Kroon, 1994). Another explanation for ridge formation is that the bars originate in the subtidal zone as subtidal bars and migrate onshore (Davis et al., 1972; Aagaard et al., 1998b). What is known is that slip-face bars form as breaker bars due to divergence of sediment transport. This is caused by the offshore transport by the bed return flow and onshore transport due to wave asymmetry (Roelvink and Stive, 1989). The decay of slip-face bars is related to high-energy wave conditions. During these high-energy events the undertow becomes the dominant process over the intertidal area resulting in a flattening of the beach (Kroon, 1994).

Low-amplitude ridges are intertidal bars without a slip-face which occur as a series of shore-parallel bars which are dissected by drainage channels (Wijnberg and Kroon, 2002; Masselink et al., 2006). The heights of low-amplitude ridges reach up to a maximum of a few tens of centimeters (Short, 1991) and the cross-shore widths reach up to a few tens of meters (Wijnberg and Kroon, 2002). Low-amplitude ridges have an asymmetric shape in onshore direction with a seaward slope of 2° to 4° (Greenwood and Davidson-Arnott, 1979; Short, 1991; Masselink and Anthony, 2001). The onshore migration rate of these bars range between 1 to 10 m/month (Mulrennan, 1992; Levoy et al., 1998; Sipka and Anthony, 1999; Stepanian and Levoy, 2003; Van Houwelingen et al., 2006). The migration of low-amplitude ridges seems to be linked to spring-neap tidal movement (Orford and Wright, 1978). The occurrence of low-amplitude ridges is characterised by flat beaches with an intertidal beach gradient of around 1° (King, 1972; Masselink and Anthony, 2001). These beaches are subjected by low to medium energy waves and have a meso- or macrotidal regime (King, 1972). The formation of low-amplitude ridges is not well understood yet. King and Williams (1949) proposed that the formation of low-amplitude ridges is probably linked to beach gradient adjustment at temporary stand-still of water during low tide and high tide. However, Simmonds et al. (1996) argued this is unlikely and the formation of low-amplitude ridges is probably related to cross-shore

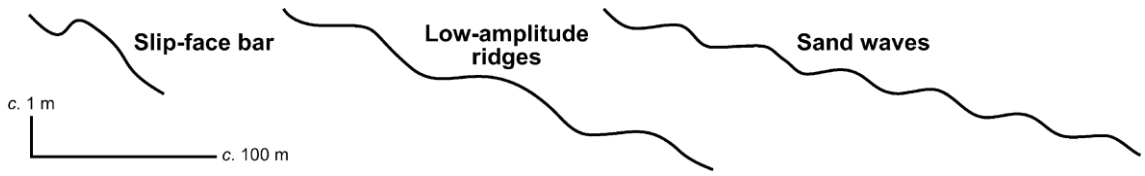

Figure 2.3. The three types of intertidal bars. (Masselink et al., 2006).

standing long waves. Low-amplitude ridges also disappear during high-energy wave conditions (King and Williams, 1949). However, the exact mechanism is not known.

Intertidal sand waves are straight or slightly sinuous features which are orientated more or less parallel to the coast. Multiple intertidal sand waves can occur on a beach ranging from 4 to 20. The height of the sand waves is in the range of several tens of centimeters and their cross-shore spacing is approximately 50 m. Sand waves do not migrate, but oscillate landward and seaward (Davidson-Arnott and Pember, 1980; Davidson-Arnott, 1981; Dawson et al., 2002). The cross-shore shape of the sand waves is symmetric with slopes ranging from 1° to 3°. The occurrence of the sand waves is characterised by a very low intertidal slope (< 0.5°) and restricted wave energy. They can be found in a wide range of tidal regimes. How sand waves are formed is still unknown. There are several suggestions like multiple wave breaking and undertow development (Exon, 1975; Dally and Dean, 1984; Dolan and Dean, 1985; Davidson-Arnott and MacDonald, 1989), standing infragravity waves (Bowen, 1980) and shoaling waves (Boczar-Karakiewicz and Davidson-Arnott, 1987).

2.1.4 Alongshore variability in intertidal beach and shoreline morphology

To determine the impact of the accretion of SPAWs to the intertidal beach it should be known what the initial intertidal beach looked like. Alongshore variability in beach morphology can also induce alongshore variability of the intertidal zone. Along the coast undulations with a nearly recurrent spacing between crests (or embayments) can be present. Due to high variety in their morphology only a rough classification can be set. The classification consists of three groups: beach cusps (Fig. 2.4), km-scale shoreline sand waves (Fig. 2.5) and mega-cusps (Fig. 2.6) (Falqués and Ribas, 2017).

Beach cusps are located in the swash zone and the embayments have a lunate shape separated by horns. The typical alongshore spacing differs between 1 and 50 meters (Coco, 2017). The formation of beach cusps is under debate, but it is most likely related to self-organisation through sediment-flow feedbacks (Werner and Fink, 1993). The beach cusps influence the dimensions of the intertidal area, because the seaward-pointing horns are relatively steep compared to the gentler sloping embayments. Beach cusp occurrence is often related to a steep beachface on reflective beaches (Masselink and Pattiaratchi, 1998).

Mega-cusps have similar shapes compared to beach cusps, but have larger alongshore spacing (100 – 1000 m). The formation of mega-cusps is related to rhythmic surf zone bars and rip channel systems (Thornton et al., 2007; Falqués and Ribas, 2017). Thornton et al. (2007) found that this relation is significantly correlated at the 95% confidence interval with a maximum cross-correlation of 0.35 at zero spatial lag. However, their shoreline and sandbar measurements were not conducted at the same moment which resulted in a limitation when determining the cross-correlation.

Sand waves have larger alongshore spacing. For the Dutch coast the alongshore spacing is between 3.5 and 10 kilometers (Ruessink and Jeuken, 2002). The formation of these features is associated with bathymetric undulations extending well beyond the surf zone (Falqués and Ribas, 2017).

Onshore migration of nearshore bars influences the hydrodynamics and therefore the morphology in the intertidal zone. During this onshore migration rip current circulations can be affected. Initially there is only a small constriction of rip channel width and an increase in rip flow velocity, but when the bars migrate further onshore the feeder currents start to fill in. When the longshore bars weld to the beach also the rip-head bar welds to the longshore bars. Therefore, sediments are now

Figure 2.4. An example of beach cusps. (Almar et al., 2008).

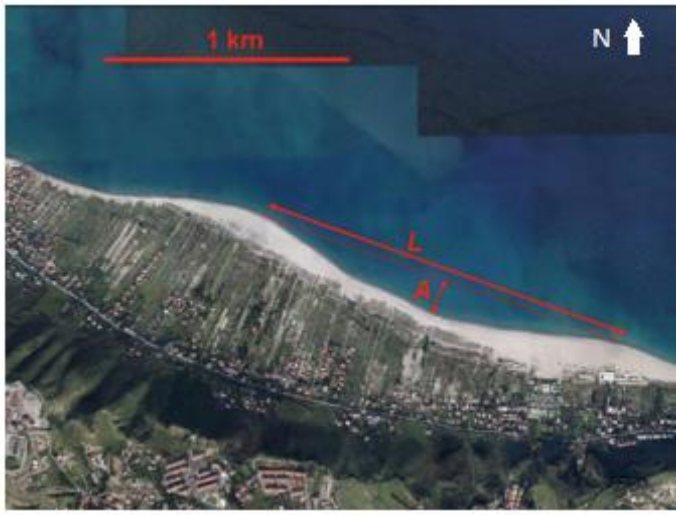

Figure 2.5. An example of sand waves. (Falqués and Ribas, 2017).

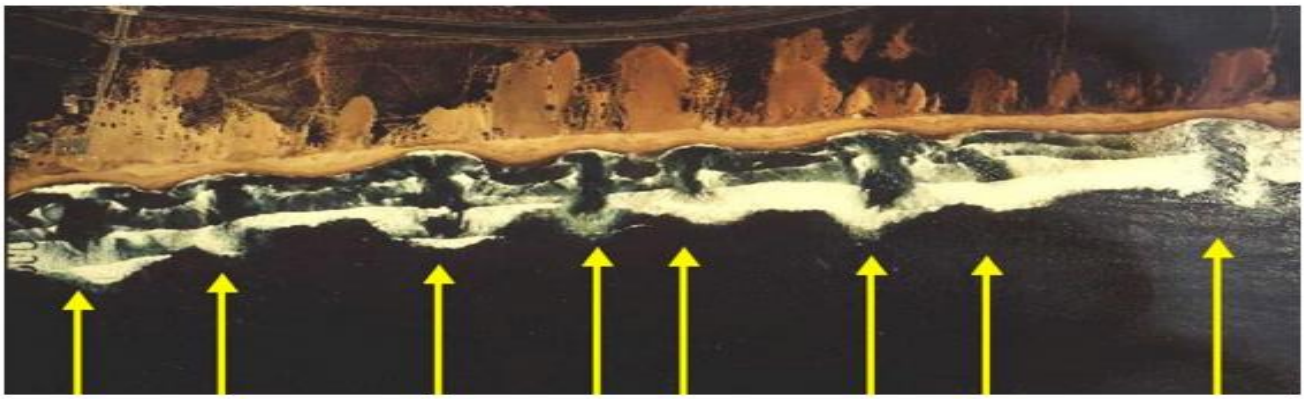

Figure 2.6. An example of mega-cusp embayments. The beach is narrower behind the rips. (Thornton et al., 2007).

transported across the bar and completely fill in the feeder currents. The rip is now constricted by the bars and the beach, and the feeder currents disappear. The main source of water for the rip current is now side-drainage off the bars (Brander, 1999). This process is similar to an up-state transition according to the beach classification system of Wright and Short (1984).

2.1.5 Sandbar-shoreline coupling

An important process determining the morphology of the shoreline is the coupling between the (inner) sandbar and the shoreline. The phase of this coupling can vary between in-phase (0°) and out-of-phase (180°). In-phase coupling means that the horn of the bar coincides with the embayment of the beach. On the other hand, out-of-phase coupling means that the horn of the bar coincides with the horn of the beach. The formation of mega-cusp embayments is an example of out-of-phase coupling (Thornton et al., 2007).

The sandbar-shoreline coupling is affected by a number of processes and physical parameters. First, the water depth along the crescentic sandbar is important. The alongshore variability in the water depth results in an alongshore variability in wave height. Due to this variability circulation patterns will be induced near the shoreline. Second, the angle of incidence is important for the phase of the shoreline-sandbar coupling. An angle of incidence between 0 and a few tens of degrees induces circulation currents which give rise to meandering alongshore currents. A larger angle of incidence results in an even stronger alongshore current. Then the sandbar is not able to maintain its crescentic shape and the sandbar and shoreline are decoupled. Third, the cross-shore distance

between the sandbar and the shoreline is important, because this affects the degree to which the shoreline reflects the sandbar pattern (Coco et al., 2005; Price and Ruessink, 2013; Van de Lageweg et al., 2013).

Related to the inner bar the shoreline mostly shows an out-of-phase coupling (Komar, 1971; Sonu, 1973; Coco et al., 2005; Thornton et al., 2007; Orzech et al., 2011; Van de Lageweg et al., 2013). Van de Lageweg et al. (2013) found that in the first three years of their research there was a strong out-of-phase sandbar-shoreline coupling during the summer months. During the winter months no or little coupling occurred. This can be related to a reduced separation distance during the summer. After those three years no summer correlation was found.

When an intertidal bar is present, coupling between the inner subtidal bar and intertidal bar can occur. Haas et al. (2003) found that under shore-normal waves rip currents can develop in the inner bar shoreward of the shoals of the outer bar, and thus an out-of-phase coupling is present. The rhythmicity of the intertidal bar was correlated to the rhythmicity of the inner subtidal bar with a correlation of 0.58. The alongshore variability of the subtidal bar determined the locations of the rip channels in the intertidal bar. The phase between the intertidal and subtidal bar varied because the bars had different migration rates. When the subtidal bar was located too close to the beach an intertidal bar was absent (Quartel, 2009).

2.1.6 Lee and feeder effect

SPAWs can be seen as small natural nourishments (Van der Weerd, 2012). Nourishments affect the hydrodynamics in the nearshore zone and these effects could also be relevant for SPAWs. The effects can be divided in cross-shore and alongshore effects. The alongshore effect (lee effect) is caused by the fact that oblique waves break over the nourishment resulting in the dissipation of wave energy. Landward of the nourishment the waves will have less energy and will result in less set-up than in the surrounding areas. This will therefore result in a less strong alongshore current. Consequently, updrift sedimentation and downdrift erosion will occur causing alongshore variability in beach width (Fig. 2.7A). The cross-shore effect (feeder effect) is caused by increased sediment transport over the nourishment. Seaward of the nourishment large waves break. The smaller asymmetric waves which did not break yet cause onshore sediment transport over the nourishment. The smaller waves shoreward of the nourishment cause less sediment transport when they break.

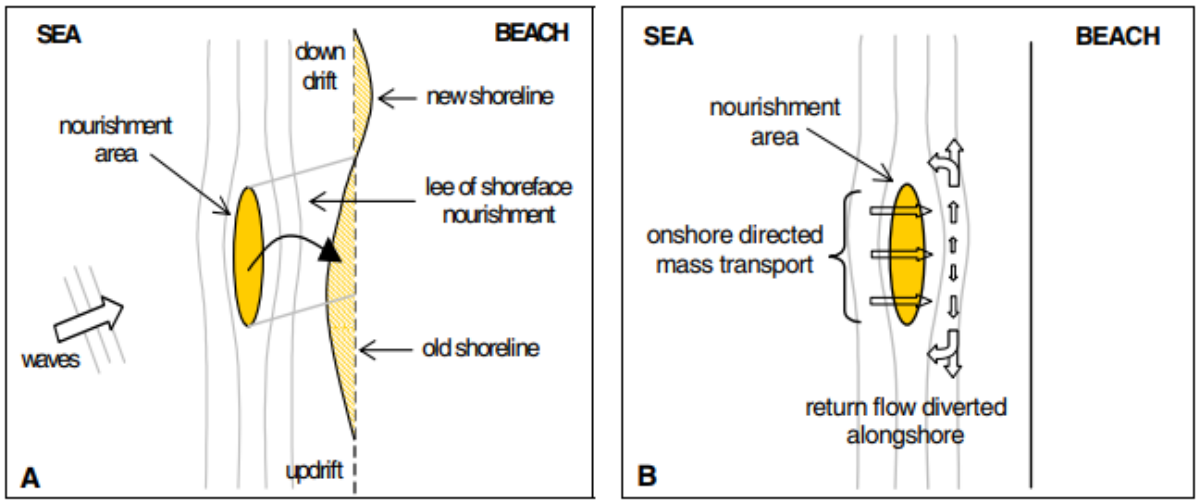

Figure 2.7. A) Alongshore effect (lee effect) of shoreface nourishments on the nearshore zone. B) Cross-shore effect (feeder effect) of shoreface nourishments on the nearshore zone. (Van Rijn and Walstra, 2004).

Also, the undertow decreases resulting in less offshore-directed sediment transport. This results in erosion on the seaward side of the nourishment and in sedimentation on the lee-side of the nourishment. Therefore, onshore propagation of the nourishment will occur (Fig. 2.7B) (Van Rijn and Walstra, 2004).

2.1.7 Connection to dune area

The intertidal area is a source of sediment for the dry beach and the dunes. Therefore, the dimensions of the intertidal area are important for the sediment flux between these areas. Wider beaches generally result in more onshore aeolian sediment transport, because the fetch is longer. However, there is a maximum beach width above which dune accretion will not further increase (Keijsers et al., 2014). Also, there are exceptions where on wider beaches the dune accretion decreases due to the presence of moist shore parallel depressions (Keijsers et al., 2014). During calm conditions the beach evolves into a more reflective beach state. A prominent berm is developed and the slope of the foreshore becomes relatively steep. During storm conditions, when beach and dune erosion occur, the beach is set back to a dissipative beach state (Wright and Short, 1984). The sediment is then deposited as intertidal and off-shore bars (Thom and Hall, 1991). In general, aeolian transport is potentially highest on dissipative beaches and lowest on more reflective beaches. This is caused by the fact that dissipative beaches are low-sloping and have numerous parallel bars and troughs. On reflective beaches the slope of the beach face is higher causing more slope disturbance. This results in a larger fetch on dissipative beaches than on reflective beaches and therefore more potential for aeolian transport (Short and Hesp, 1982). The evolution of the dune shows a correlation with bar migration and alongshore variation in beach state on a decadal scale (Guillén et al., 1999).

The width of the intertidal area can be influenced by the welding of near-shore bars to the beach. This locally increases the width of the beach and therefore also increases the fetch length. The welding to the beach also results in a larger availability of sediment for aeolian sand transport. Therefore, there is more sediment available for transport to the foredune (Aagaard et al., 1998a; Christiansen and Davidson-Arnott, 2004). The welding of a nearshore bar occurred at the Skallenger barrier, Denmark, (Aagaard et al., 2004) and at Calais, France (Anthony et al., 2006). Aagaard et al. (2004) and Anthony et al. (2006) found that the increase in beach width resulted in an increase of dune accretion. At Skallenger, the increase in beach width resulted in higher aeolian sand transport from the beach to the foredunes with moderately strong winds (Fig. 2.8). After a storm the intertidal bar was removed and consequently the intertidal beach width decreased which resulted in less sediment transport.

High wind velocities are often related to storm conditions which mean that high water levels coincide with high wind velocities. As a result, only a small part of the beach is available for aeolian transport. Therefore, aeolian transport is only reasonable when the intertidal bar had welded to the beach enlarging the backshore (Christiansen and Davidson-Arnott, 2004). It should be noted that at the Dutch coast the sandbars generally migrate offshore (e.g. Ruessink and Kroon, 1994; Wijnberg and Terwindt, 1995). However, the accretion of a SPAW could induce higher aeolian sediment transport and thus locally more dune accretion.

On beaches with a complex intertidal bar-trough morphology the morphology influences the wind flow patterns over the intertidal beach. The wind speed tends to decrease in the trough because of

air expansion. Troughs also have a higher moisture content and therefore the mobilization of sediment is prevented and sediment is trapped. Especially, the high moisture content in the troughs is important for cross-shore sediment transport. The occurrence of these wet troughs limits the dry fetch, because the beach is segmented in wet and dry zones. Also, the presence of bedforms can limit the aeolian sand transport. Especially, the part of the beach located close to the dunes is important for the sediment flux between the beach and the dunes. When the most shoreward trough is located close to the foredune the sand supply can be considerably constricted. The ideal situation for cross-shore sediment transport from the beach to the foredune occurs when the wind is directed onshore from an oblique angle, which lengthens the fetch, during neap tide (Anthony et al., 2009).

Dune erosion is caused by wave action during storm events. A wider beach will result in more wave dissipation before the waves reach the dunes. Therefore, less wave energy will rework the foredunes and less erosion will take place (Ruessink and Jeuken, 2002). Moreover, the presence of an intertidal bar reduces the wave energy available for dune erosion, because waves break over these bars (Masselink et al., 2006). Alongshore variability in beach width can result in an alongshore variability in dune erosion. Thornton et al. (2007) found that the alongshore variation in the shoreline and alongshore variations in dune erosion are significantly correlated at 95% confidence with a maximum correlation of 0.40. The accretion of a SPAW to the beach would result in a local increase of beach width shoreward of the former horn of the bar. The increase in beach width could result in less erosion of the dunes shoreward of the place of SPAW accretion.

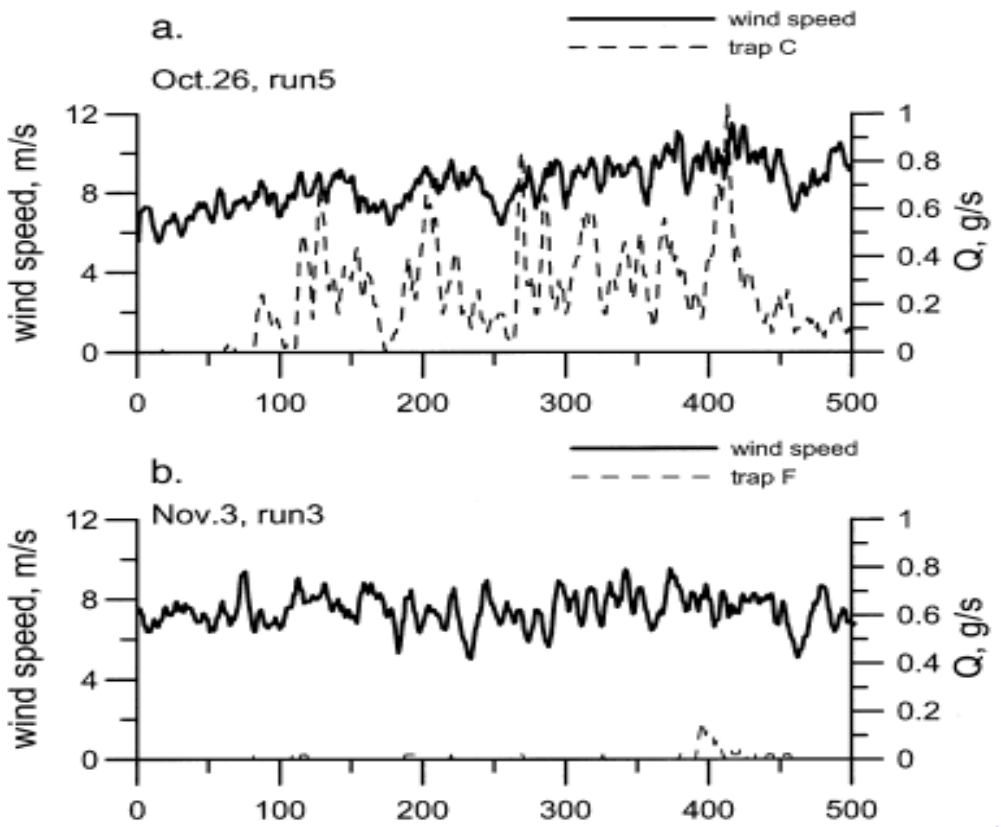

Figure 2.8. Instantaneous measurements of wind speed and aeolian sediment transport (Q) at the base of the dune ramp (a) prior to and (b) after a storm surge and intertidal bar removal. (Aagaard et al., 2004).

2.1.8 Relation to SPAWs

To understand the effect of SPAWs on the intertidal beach it is important to know how the intertidal beach looked before the emergence of a SPAW. Often the inner sandbar shows coupling to the shoreline. This coupling is linked to certain circulation currents which are present near the coast. These circulation currents already induce the formation of mega-cusps near the coast. Other processes could induce the formation of beach cusps and sand waves. These processes already induce an alongshore variability of the shoreline. So, to determine the impact of a SPAW on the intertidal beach the initial shape of the shoreline should be taken into account. This is also the case for the intertidal beach because the shape of the intertidal beach will be affected by the large input of sand which could have an effect on the dimensions of the intertidal bar system.

The emergence of a SPAW and the welding of a SPAW to the beach affect the hydrodynamics and morphodynamics at the beach. SPAWs show similarities with nourishments and it is known nourishments induce circulations in the nearshore. Therefore, these processes could also be important when a SPAW migrates to the beach. Moreover, the emergence of a SPAW changes the beach profile. This affects the wave processes acting along the beach profile because when the water depth is low enough, waves will break over the SPAW. The welding of a SPAW to the beach will locally increase the beach width which enlarges the fetch. As a result, the aeolian transport will increase and the sediment transport to the dune system will be larger.

2.2 SPAWs

2.2.1 Definition

SPAWs are documented and named by Wijnberg and Holman (2007), although these features were already mentioned by Greenwood and Davidson-Arnott (1975), Konicki and Holman (2000) and Shand (2007). Wijnberg and Holman (2007) defined a SPAW as a small bar-like feature that has shed from the shoreward side of a sandbar, which then propagates through the trough as an intact feature and subsequently merges with the beach (Fig. 2.9). In multi-barred systems SPAWs can also migrate from an outer bar to an inner bar (e.g. Almar et al., 2010; Price et al., 2017). The feature is called a wave, because it is a single, isolated perturbation that maintains its shape while propagating, just like a solitary wave (Wijnberg and Holman, 2007).

2.2.2 Formation

The evolution of a SPAW can be divided in three processes: the formation, the migration and the welding to the beach/bar (Fig. 2.10). Wijnberg and Holman (2007) defined the moment that the

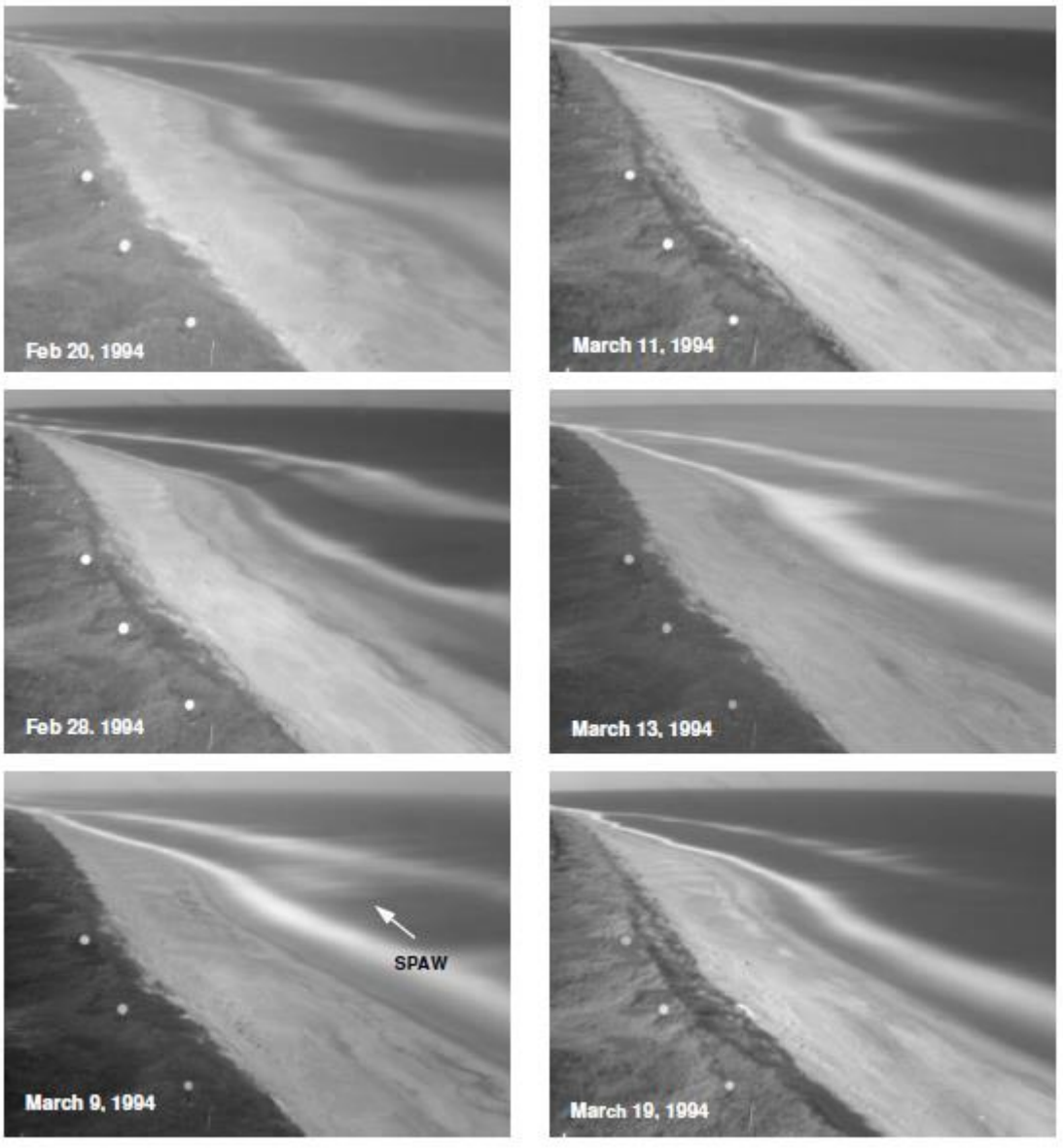

Figure 2.9. Sequence of time-exposure images at Duck capturing a SPAW event. (Wijnberg and Holman, 2007).

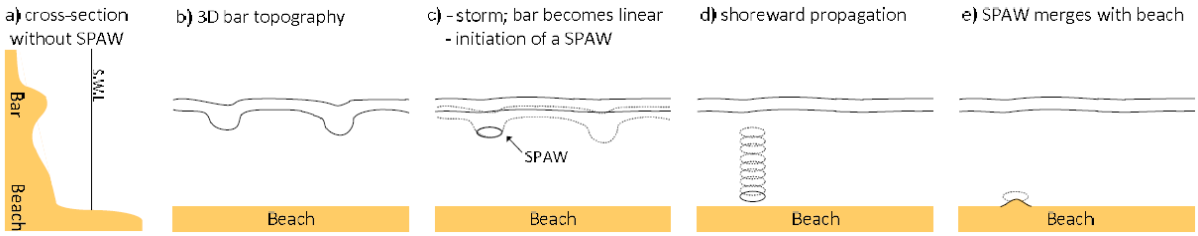

Figure 2.10. Conceptual sketch of the formation, migration and welding to the beach (or an inner bar) of a SPAW. (a) Cross-section without a SPAW. (b) 3D bar topography before the formation of a SPAW. (c) Formation of a SPAW. (d) Migration of a SPAW from a bar to the beach (or an inner bar). (d) Welding of the SPAW to the beach (or an inner bar). (Van der Weerd, 2012).

SPAW separates from the bar as the starting point of the SPAW. The processes resulting in the formation of a SPAW are still poorly understood. The formation of SPAWs seems to be linked to a 3D bar pattern and high wave conditions (Almar et al., 2010; Price et al., 2017). During a storm the bar pattern is generally smoothened (Van Enckevort et al., 2004), but at beaches with a crescentic bar pattern the most shoreward part of the horn can separate from the bar and form a SPAW (Wijnberg and Holman, 2007; Almar et al., 2010; De Wit, 2017; Price et al., 2017). It is also possible that a SPAW forms when during a bar bifurcation a part of the bar disconnencts (Shand, 2007; Price et al., 2017). In a modelling study of Castelle (2004) a feature similar to a SPAW was obtained. The feature emerged because of degeneration of the horn and was only found with high energetic waves and a well-developed crescentic bar pattern. At Duck (USA), SPAWs occurred approximately 2 times per year (along 800 m of beach) (Wijnberg and Holman, 2007). The largest amount of SPAW events occurring in Duck in one year was 5. Near Egmond aan Zee (The Netherlands), hereafter referred to as Egmond, 6 to 7 SPAW events occurred each year between 2001 and 2014 with a maximum of 15 in 2014 (along 4000 m of beach). In 14 years 41 SPAWs emerged from the outer bar and 52 from the inner bar (Price et al., 2017).

2.2.3 Migration

Once the SPAW is disconnected from the bar it transits the trough to an inner bar or the beach. At Duck propagation speeds between 1.7 m/day and 4.8 m/day occurred with an average of 3.1 m/day. The standard deviation found was 0.8 m/day. The duration of the SPAW events differed greatly. On average, it took 17 days before the SPAW welded to the beach with a minimum of just a week, a maximum of up to 7 weeks and a standard deviation of 9 days (Wijnberg and Holman, 2007). At Egmond the average SPAW duration was approximately 40 days (Price et al., 2017) and at Truc Vert Beach (France) it took only one day for the SPAW to cross the trough (Almar et al., 2010). It should be noted that the duration of a SPAW event also relates to the distance between the bars. Also, at Egmond it was found that during the more energetic (winter) months it occurred that SPAWs were eroded during their migration (Price et al., 2017). The SPAW event studied by De Wit (2017) showed that the cross-shore migration was incremental. The SPAW reached the trough in seven days, but remained there for approximately 45 days. Eventually, the SPAW migrated further to the inner sandbar during high wave conditions (De Wit, 2017). It should be noted that Almar et al. (2010) and De Wit (2017) only studied one SPAW which could possibly not be representative for the area.

At Truc Vert Beach a SPAW migrated from the outer bar to the inner bar (Almar et al., 2010). The alongshore position of the SPAW remained nearly constant despite the high energy oblique waves. Also, the SPAW did not migrate alongshore during a storm while this was the case for the outer bar horns and the rip channels. In the following calmer period the intertidal bar (shoreward of the SPAW)

migrated alongshore, but again the alongshore location of the SPAW remained constant. This indicated that the SPAW is an independent feature in the system (Almar et al., 2010). On the other hand, near Egmond SPAWs did show alongshore migration (3 to 8 m/day) which did correspond to high wave events (De Wit, 2017).

2.2.4 Dynamics

Van der Weerd (2012) performed a modelling study to determine the dynamics of a SPAW and its influence on the hydrodynamics. For the base case (H_s = 0.56 m, T_p = 8.2 s and z = 0 m) a schematized bathymetry was used which was based on a SPAW event at Duck. Waves broke over the SPAW and therefore wave heights differed alongshore. This variation in breaking resulted in variations in cross-shore and alongshore radiation stress which caused local set-up and set-down. Therefore, a horizontal circulation current developed around the SPAW. Around the tips of the SPAW the current was directed offshore and over the crest of the SPAW the current was directed onshore. It was also found that the presence of the SPAW changed the sediment transport pattern, because the SPAW forced the waves to become more skewed and asymmetric. As a result, the sediment transport over the SPAW was onshore. The seaward part of the SPAW showed erosion while on the shoreward part of the SPAW accretion took place, resulting in an onshore movement of the SPAW. A remarkable result was that during low wave conditions the onshore sediment transport due to wave deformation dominated over the onshore sediment transport due to the horizontal circulation current (Van der Weerd, 2012).

In the modelling study of Van der Weerd (2012) several conditions were changed compared to the base case. First of all, the water level was changed. A reduction in water level did result in a stronger circulation current. However, the change in sediment transport was small. Variation in the cross-shore location of the SPAW between the bars resulted in a stronger circulation current when the SPAW was close to the bar and a weaker circulation current when the SPAW was close to the beach. Therefore, the sediment transport patterns were also different. For the case with a SPAW located near the bar the sediment transport was higher on the full length of the crest while for the case with a SPAW close to the beach the sediment transport was concentrated around the tips of the SPAW. The dimensions of the SPAW were also altered to a case with a wider SPAW and a case with a longer SPAW. For the case with the wider SPAW the horizontal circulation current became stronger while for the case with a longer SPAW the horizontal circulation current focussed around the tips. The stronger current and therefore higher sediment transport at the tips of the SPAW had hardly an effect on the morphodynamics. Lastly, a case with a locally lower bar seaward of the SPAW was used. In this case the depth average velocities were different than for the base case because they were mainly directed through the depression in the lowered bar. On the places where the bar had its original height the sediment transport increased. The flow pattern around the SPAW also differed. At the tips of the SPAW the flow was slightly directed to the middle of the SPAW while a horizontal circulation current was generated slightly landward of the SPAW. This could be an explanation for the relatively stable shape of the SPAW during migration (Van der Weerd, 2012).

2.2.5 Dimensions

Wijnberg and Holman (2007) used the width and length of the foam patch in the video images obtained with the ARGUS video monitoring system to define the dimensions of the SPAW since this is a proxy measure for the submerged SPAWs. The location of the SPAW was determined by measuring the distance between the crest of the SPAW and the landward inner bar/beach (Fig.

2.11A). At Duck the average length of the SPAWs was 126 m with a maximum of 255 m and a minimum of 40 m. The standard deviation for the SPAW length was 60 m. The width of the SPAWs showed less variation with a minimum of 18 m and a maximum of 58 m. On average the width of a SPAW was 30 m with a standard deviation of 10 m. During a bathymetric survey a SPAW was registered by accident. Therefore, the SPAW height could be determined for that event. The trough-crest distance was 0.7 m which was similar to the bar it originated from. No data were available to determine the evolution of the SPAW height. The SPAW remained its horizontal shape during the migration (Wijnberg and Holman, 2007). At Egmond the mean SPAW length (alongshore) and width (cross-shore) were approximately 200 m and 30 m, respectively (Price et al., 2017). These dimensions were also based on time-exposure images from the ARGUS video monitoring system. Furthermore, De Wit (2017) and Price et al. (2017) studied a SPAW at Egmond with the help of bathymetric maps based on time-exposure images and an initial bathymetric map. The average length, width and height of this SPAW were 300 m, 70 m and 0.7 m, respectively. An increase in width (50 m to 83 m), length (240 m to 360 m) and height (0.63 m to 0.71 m) was seen while the SPAW propagated to the inner bar (De Wit, 2017). The SPAW at Truc Vert Beach had a maximum length of 250 m which reduced to 100 m. This indicated that the SPAW eroded with ~5 m/day (Fig. 2.11B) (Almar et al., 2010). Remarkably, differences in evolution of the shape of the SPAWs were present for different beaches. It should be noted that the definition of the dimensions of the SPAWs differed per study and this should be considered when comparing the different SPAW dimensions.

From the dimensions discussed above, the volume of a SPAW was calculated. The average volume of a SPAW at Duck was roughly 1900 m³ (assuming the average height was 0.5 m) (Wijnberg and Holman, 2007). The corresponding onshore sediment flux was 1 to 2 m³/m/day which was similar to the onshore sediment flux found in the modelling study of Van der Weerd (2012), namely 1.3 m³/m/day. At Egmond this resulted in a mean SPAW volume of 14,700 m³ (based on assimilation model results) which was considerably higher than at Duck (Price et al., 2017). At Truc Vert beach an even higher volume of 30,000 m³ was found (Almar et al., 2010). The SPAW event studied by De Wit (2017) had an average volume of 11,000 m³ according to the results of the assimilation model. The volume just after initiation was 7,500 m³ and increased to 15,800 m³ at the end. However, when the volume was calculated from the time-exposure images the average volume was only 6,000 m³. This large difference indicates that it is hard to compare the different extraction techniques. One cause for this difference lay in the extraction of the dimension from the bathymetric maps. A certain threshold related to the edges of the SPAW must be selected to determine the dimensions, but this threshold was very sensitive. Another reason was that the method of determining the dimension

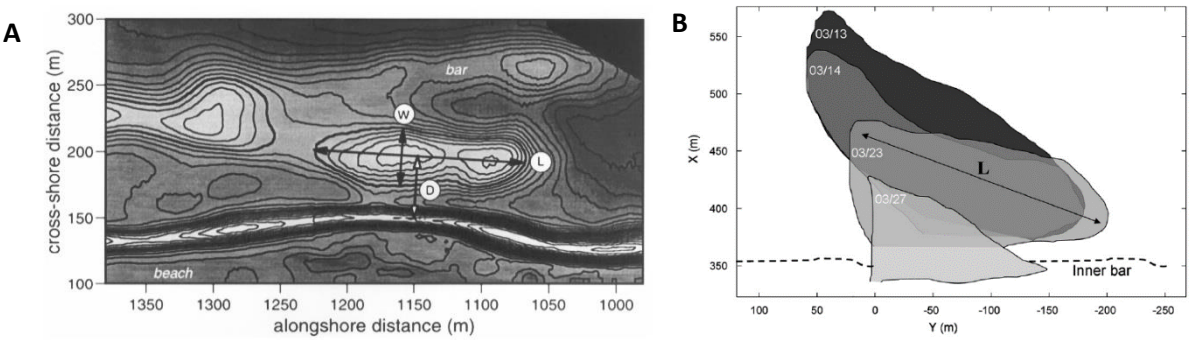

Figure 2.11. A) Definition of the dimension of a SPAW. W = SPAW width, L = SPAW length, D = SPAW initiation distance. (Wijnberg and Holman, 2007). B) Definition of maximum length of a SPAW. L = SPAW length. Note the shape change of the SPAW over time. (Almar et al., 2010).

from time-exposure images was also flawed (De Wit, 2017). The pixel intensity was only high for the parts of the SPAW where breaking occurs. This could be seen as foam in the images, but on the deeper parts of the SPAW, where no breaking occurs, the foam was absent causing an underestimation. Further improvement is needed to determine the exact dimensions of a SPAW which can be used to calculate its real volume.

2.3 Research objective & questions

The research of SPAWs is a relatively new field of interest. The features were already mentioned by Greenwood and Davidson-Arnott (1975), Konicki and Holman (2000) and Shand (2007), but the first to really document these features were Wijnberg and Holman (2007). After the study of Wijnberg and Holman (2007) SPAWs only received little attention (i.e. Almar et al., 2010; Van der Weerd, 2012; De Wit, 2016; Van Kuik, 2016; Price et al., 2017). These studies mainly focused on the dynamics of these features. The influence of the welding of these SPAWs to the beach on the beach dynamics is not studied yet and therefore poorly understood. Therefore, the objective of this research is to characterize the influence of a SPAW on the intertidal beach morphodynamics. The welding of SPAWs to the beach influences the beach dimensions. This change in beach dimensions results in a change in morphological processes acting on the beach. The increase in beach width due to welding of the SPAW to the beach locally increases the beach width and volume. The increase in sediment availability and fetch of the beach are expected to result in more aeolian transport. Therefore, it is expected a part of the sand of the SPAW is transported to the higher parts of the beach. Because the increase in beach width is only local, it is also expected the alongshore currents will disperse the sand alongshore. As previously discussed, the increase in beach width may locally also result in less dune erosion during storms. However, the effect of a SPAW event may not only be limited to the period after the SPAW welded to the beach. During its migration phase the SPAW can induce its own circulation current and because of the lee effect it could already affect the beach width and its alongshore variability. To fulfil the objective above, the research is divided in the following questions and sub questions:

- How does a SPAW event influence the characteristics (width, volume, alongshore variability and morphology) of the intertidal beach compared to areas alongshore without SPAW events?
    - What is the effect of the SPAW on the intertidal beach characteristics in the period between SPAW emergence and SPAW welding?
    - What is the effect of the SPAW on the intertidal beach characteristics in the period after SPAW welding?
- How does the sand of a SPAW disperse in cross-shore and longshore direction?
    - How is the sand of the SPAW redistributed (cross-shore and alongshore) in the period before and in the period after the SPAW welded to the beach?
    - At what rate does the sand disperse (cross-shore and longshore)?
    - How long does it take before the influence of a SPAW event on the intertidal beach is no longer present?

Chapter 3 Study area and data collection

3.1 Egmond aan Zee

This study focusses on the beach near Egmond aan Zee, The Netherlands. Egmond aan Zee is located at the central part of the Dutch uniform coast (Fig. 3.1). The beach is approximately north-south orientated and is backed by an extensive dune area with dunes reaching up to 25 meters. The dunes are covered with European marram grass (*Ammophila arenaria*). The intertidal beach is relatively flat (≈ 1:30) and has a median grain size D_{50} of 0.25-0.30 mm (Aagaard et al., 2005; De Winter et al., 2015). The median grain size decreases offshore to 0.2 mm in the outer nearshore (Aagaard et al., 2005). Egmond is a multi-barred beach with generally two subtidal bars and one intertidal bar. The intertidal bar is an intertidal slip-face bar. This means the intertidal bar has a landward facing slip-face and a pronounced elevation difference between the trough and the crest of more than 1 meter. The landward slope of the intertidal bar is quite steep with values up to 30-35° while the seaward slope is flatter with values of 3-6° (Masselink et al., 2006). According to the beach classification of Masselink and Short (1993) the beach at Egmond belongs to the intermediate group, roughly at the transition of the subgroups 'barred beaches' and 'low tide bar/rip'. The water depth on the crests of the subtidal bars is 2 m and 4 m (in 2005) (Price and Ruessink, 2008). The subtidal bars are steep with deep intervening troughs (Aagaard et al., 2005). The crescentic pattern of the inner bar often has an alongshore spacing of 200-500 m (Van Rijn et al., 2002). The intertidal beach width ranges from approximately 50 to 100 m and has quasi-rhythmic intertidal bars and intervening rip channels (Aagaard et al., 2005).

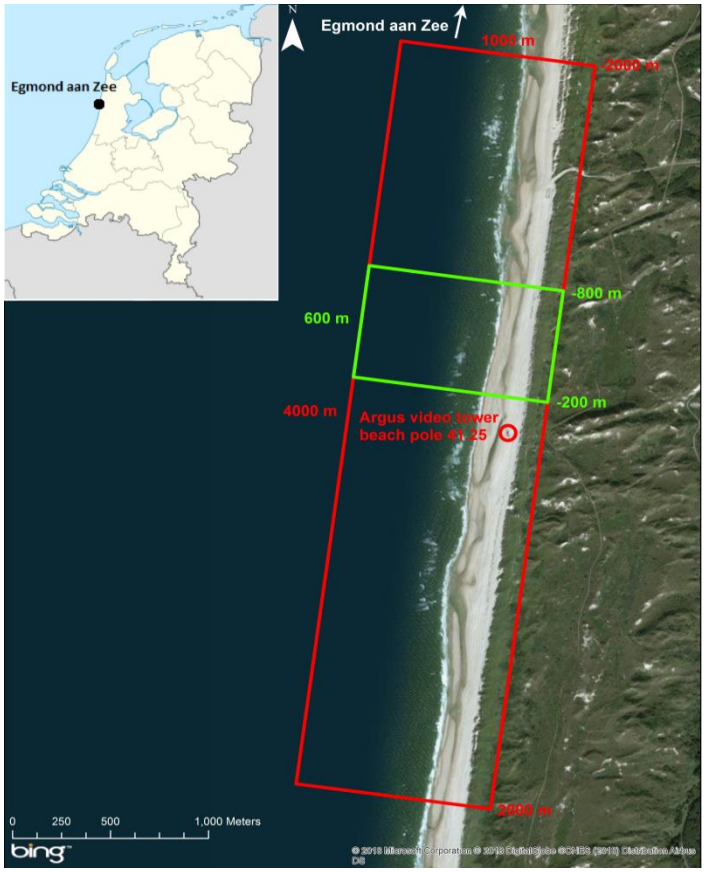

Figure 3.1. The location of the study site. The red box covers the area where the ARGUS video tower collects images. The green box covers the study area in which the SPAW event will be analyzed.

The beach is wave-dominated and mainly exposed to sea waves which are generated on the North Sea (De Winter et al., 2015). Most of the waves come in from the southwest to north (Aagaard et al, 2005). For the period between 1999 and 2011 the significant wave height H_s and peak period T_p were registered by a near-by buoy located in about 26 m depth. H_s and T_p were 1.3 m and 5.9 s, respectively. During north-westerly storms the H_s and T_p can increase to over 7 m and 12 s, respectively. Also, the water level increases by 0.5 – 1.5 m during storm conditions. However, storm events where the water reaches the dunes are rare (De Winter et al., 2015).

The tidal regime is micro-tidal, semi-diurnal and asymmetric. The tidal range ranges from 1.4 m during neap tide to 2.0 m during spring tide. The rising period of the tide lasts 4 hours while the falling period of the tide lasts 8 hours. The alongshore currents induced by the tide show a net tidal current in northward direction, because of a larger flood current. The tidal current can reach up to 0.5 m/s (Price and Ruessink, 2008).

3.2 ARGUS video data

3.2.1 ARGUS video system

The development of the Argus video technique was initiated by the group of Prof. Rob Holman (Coastal Imaging Lab, Oregon State University, USA) in 1984. The objective was to develop a system which could monitor for a long period with low costs to study coastal zone management problems. In 1986 large field campaigns were held at Duck (USA) to test the system. In 1991 the first completely unmanned video station was installed and in 1992 when the first totally automatic system was placed the system was named Argus, referring to a mythical Greek creature with 100 eyes (Aarninkhof, 2004; Holman and Stanley, 2007). The Argus tower at Egmond was placed in December 1997 (Holman and Stanley, 2007), but was taken out of use in 2015.

An Argus system consists of a field station and an archive station. The field station consists of 5 cameras which cover a 180^o field of sight. There are also some hardware components present related to the connection of the cameras and the computers. The data are then sent to the archive station which is located at a company/university. Normally, the Argus video station captures three types of images: snapshots, 10-minute time-exposure images (timex images) and variance images (Fig. 3.2). During day time these images are collected every 30 minutes. The snapshot is not used for quantitative analysis, but can be used to determine the quality of the images. The time-exposure image is constructed by averaging all the images collected during 10 minutes with a frequency of 2 Hz. This type of image is especially used for analysis. Because the image is averaged over time, moving features like people and individual waves are removed. Features which do not move over time remain in the image (Holman and Stanley, 2007). A very useful application of the timex image is

Figure 3.2. A) Snapshot. B) Time-exposure image. C) Variance image.

that preferred wave breaking in the surf zone results in white bands (foam). This indicates the locations of sandbars and rip currents (Lippmann and Holman, 1989). The variance image is actually an image with standard deviations. The image displays the standard deviation of the pixel intensities of the images collected in the same 10 minutes. A high standard deviation means the intensity of the pixel varies over time. This is for example the case in the surf zone due to wave breaking. Low values will be present on the beach when no/little change occurs in 10 minutes. These images are often used to determine the location of the surf zone and wave breaking (Holman and Stanley, 2007). The Argus system could be used to study seasonal fluctuations in beach width, the development of nourishments, dune erosion during storms and the morphological impact of hydraulic structures.

At Egmond aan Zee the whole area covered by the Argus video tower reaches 4000 m alongshore, but the area in which the SPAW event will be studied spans 600 meters alongshore from -200 meter to -800 meter (Fig. 3.1). The area covered by the Argus video tower will be referred to as the Egmond coast and the area in which the SPAW was studied will be referred to as the study area. The ARGUS imagery used to study the evolution of SPAWs in this study was recorded in the period between June 2014 and September 2015. Unfortunately, multiple days were not (fully) recorded or even not available. This is the reason there are no data between 12 December 2014 and 6 April 2015.

3.2.2 BarLine Intensity Mapper (BLIM)

For this research barlines extracted with the BarLine Intensity Mapper (BLIM) were also provided which could be used to study the impact of SPAWs on the shoreline. For the extraction of the barlines, images from the ARGUS video monitoring system were used. These images were then merged into plan view images. On these images continuous high-intensity bands were visible which can be a reasonable estimate for submerged sandbars (Lippmann and Holman, 1989). By tracking the alongshore maximum intensity value sand bars could be identified. The BLIM algorithm was originally developed by Van Enckevort and Ruessink (2001). In the algorithm the maximum intensity value is determined for each vertical row within a certain region. Then the vertical positions of these pixels are smoothed. This will result in a continuous smooth maximum intensity line alongshore. In the BLIM toolbox the option to add a region of interest (ROI) was added for better results. Now distracting features could be excluded from classification (Pape, 2008).

The most shoreward located barline often corresponded to the shoreline (low tide line). This was useful because the barlines were available for each day. Therefore, there was continuous shoreline data which was not the case for the shoreline data collected with the IBM. This made it easier to determine the impact of a SPAW on the beach. However, on some days the most shoreward barline was located more shoreward than expected. This often corresponded to high wave conditions. Then the most shoreward barline did not correspond to the low tide level, but to the location of the water level at that time. If possible the most shoreward barline was then switched for the second most shoreward barline which was more likely to represent the low tide level on these days. The pixel size of the plan view images used for the barline classification was 2.5 by 2.5 m and the barlines were collected along the whole area covered by the Argus video tower (4000 m).

3.3 Wave and tide data

To determine the shoreline elevation from the timex images wave and tide data were needed. The offshore root mean square wave height H_{rms}, peak period T_p and the angle of wave incidence θ were collected hourly by a wave buoy located approximately 15 km south of Egmond, named 'IJmuiden

munitiestortplaats'. When wave data were missing the data were replaced with data from a wave buoy ('Eierlandse gat') approximately 75 km to the north. Offshore water level data were obtained by two tidal stations which were located 15 km north and south of Egmond (Aarninkhof et al., 2005). The wave heights and wave directions used in the analysis were also measured at the tidal station 'IJmuiden munitiestortplaats'.

3.4 Topographic data

The data used for the validation of the interpolated bathymetries were collected with a MLS (Mobile Laser Scanner) system attached to an internal navigation system with a RTK-GSP (Real-Time Kinematic Global Positioning System). With this system 10 surveys of a 3-km beach stretch between Castricum and Egmond aan zee were conducted. One of these surveys was conducted on 10 October 2014 which was during the period of this study. The amount of measurement points collected per m^2 depended on the surface slope and the distance from the MLS, but typically varied between 300-100. The height observations were then mapped into 1x1 m DEMs (Digital Elevation Models). To determine the quality of the MLS-generated DEMs, they were compared to manually collected RTK-GPS measurements. It was found the error increased further away from the system, but remained within the specified accuracy of 0.2 m at 100 m from the car (Donker et al., 2016).

Chapter 4 Extracting intertidal beach characteristics from video data

4.1 Shoreline detection methods

To determine the dimensions of the intertidal area the shoreline for each image should be mapped. In earlier studies four methods were developed to extract the shoreline: the SLIM model (Plant and Holman, 1997), the PIC model (Aarninkhof and Roelvink, 1999; Aarninkhof, 2003), the ANN model (Kingston, 2003) and the CCD model (Turner et al., 2001). The elevation corresponding to the shoreline was calculated by a water level model which will be discussed later in section 4.2.2.

SLIM model (Shore Line Intensity Maximum model)

The SLIM (Shore Line Intensity Maximum) model makes use of the foam production of the swash. If present, the foam will be visible as a parallel band of high-intensity in the timex images and is named the SLIM. This method was developed at Duck. At this site the beach slope is relatively steep and narrow resulting in a well-defined swash zone. As a result, the SLIM is almost always visible. The shoreline position is determined with the help of quadratic and Gaussian functions. A superposition of these functions is plotted over the intensities over a cross-shore transect. The maximum of the function is the shoreline position. The root mean square elevation error is around 0.1 m (Plant and Holman, 1997).

PIC model (Pixel Intensity Clustering model)

The PIC (Pixel Intensity Clustering) model, also known as IBM (Intertidal Beach Mapper), was developed because the SLIM model did not work on the more dissipative Dutch coast. The presence of intertidal sandbars would result in multiple shorelines cross-shore. The shorelines landward of the intertidal bar would not have swash and therefore no SLIM. The PIC model makes use of the spectral information of the image. First, the red, green and blue bands (RGB) are converted in hue, saturation and intensity value bands (HSV). Hue and saturation reflect the colour information while the intensity value reflects the greyscale intensity. In general, the beach has two main components: sand and water. The different spectral properties of these components are used to differentiate between them and so determine the shoreline location (Aarninkhof, 2003). This method will be discussed in more detail in section 4.2. The root mean square elevation error corresponding to this technique is 0.2 m (Aarninkhof et al., 2003).

ANN model (Artificial Neural Network model)

The ANN (Artificial Neural Network) model was also developed because the SLIM method was not able to correctly operate on dissipative beaches. Also, this technique was developed to deal with more complex geometries, like partially submerged sandbars, spits and inlets. The technique makes use of a neural network to differentiate between wet and dry pixels. For this method training images have to be manually classified. The corresponding RGB values are used as input for the unclassified images. All pixels are classified as a 0 (water) or 1 (sand). An intermediate classification value, which was unlikely to be sand or water, was selected to be the shoreline. The elevation error is around 0.2 m (Kingston, 2003).

CCD model (Color Channel Divergence Model)

The CCD (Color Channel Divergence) model is based on the difference between the spectral properties of water and sand. This model was also developed, because the SLIM model failed on dissipative beaches. Water and sand have different reflectance in red and blue. On the beach all intensities are similar, because of the white sand on the beach. However, more shoreward the intensities first drop because of darker wet sand and then diverge because water reflects more blue than red. This change in red and blue intensities is determined over a cross-shore transect. To determine the shoreline a divergence threshold is selected. This threshold can be selected by calibration with bathymetric survey data (Turner et al., 2001).

Plant et al. (2007) studied the performances of these four models on a variety of coasts. All methods gave an offset in shoreline position which differs for each study site. The PIC, ANN and CCD methods resulted in a relatively large offset of the shoreline position in shoreward direction. This offset was caused by the swash and surfbeat (Plant et al., 2007). On the other hand, the SLIM model resulted in an offset in seaward direction caused by variations in the surf similarity parameter (Plant and Holman, 1997). The CCD model tended to fail on beaches with unusual sand colour. For example, the sand at the Teignmouth site had a reddish colour. This problem could probably be tackled by using a different colour discrepancy. The PIC and ANN model classify individual pixels. Therefore, shorelines at coasts with complex intertidal morphology can be determined. As a result, the hydrodynamic interactions may be more complicated leading to larger elevation errors (Plant et al., 2007).

In this study the shorelines will be determined at Egmond. The PIC model was developed for Egmond and therefore gave relatively good result. When looked at the root mean square error (RMSE) the PIC model showed the best results at the Egmond coast (RMSE = 0.17 m). The SLIM (RMSE = 0.44), ANN (RMSE = 0.20) and CCD (RMSE = 0.35) models all showed larger errors (Plant et al., 2007). Therefore, the PIC model will be used in this study.

4.2 Intertidal Beach Mapper (IBM)

The PIC model, hereafter named IBM (Intertidal Beach Mapper), showed the best result for the Egmond study area. The IBM is embedded in the Argus runtime environment. The IBM consists of two parts: the shoreline detection model and the shoreline elevation model (Fig. 4.1). The shoreline detection model determines the location of the shoreline based on differences in pixel intensity between sand and water. This will be further explained in section 4.2.1. The shoreline elevation model determines the vertical elevation of the shoreline from the hydrodynamic conditions offshore. This will be further explained in section 4.2.2. These shorelines are collected during different stages of the tide. Therefore, the intertidal bathymetry can be determined from these shorelines (section 4.4).

4.2.1 Shoreline detection model

The 10-minute time exposure images obtained by the Argus video monitoring system were collected as raw image intensities in a 'Red-Green-Blue' (RGB) colour space. The data were obtained in a manually determined region of interest (ROI) which should contain both the sea and the beach. The raw image data were then converted to a 'Hue-Saturation-Value' (HSV) colour space. This was done to separate colour information (Hue and Saturation) from grey scale information (Value). The image intensities were then filtered to remove outliners and scaled to values between 0 and 1. The

shoreline was determined by making use of the contrast between dry and wet pixels and therefore an iterative low-pass filter was used to filter the spiky histogram into a smooth histogram with two well pronounced peaks P_{dry} and P_{wet}. These peaks indicated the locations of the clusters of dry and wet pixels. To determine the boundary between wet and dry pixels a line l was defined, which is formulated as:

$$l: I_y = p_1 I_x + p_2 \tag{4.1}$$

where in the case of colour-based discrimination I_y represents Hue and I_x represents saturation. However, when the luminance-based discrimination is used I_y and I_x both represent value. Which method was used to determine the shoreline was based on the highest degree of contrast between sand and water. This was done by relatively measuring the spread of pixel intensities within each cluster regarding to the distance between the cluster peak P and the discrimination line l. A discriminator function $\Psi(I_x, I_y)$ was defined such that $\Psi=0$ along l:

$$\Psi(I_x, I_y) = p_1 I_x + p_2 - I_y \tag{4.2}$$

Now a map of the function Ψ could be generated. The negative values represented the submerged parts of the beach while the positive values represented the dry parts of the beach. The shoreline feature in the image space was the Ψ = 0 elevation contour (Aarninkhof et al., 2003). The shoreline was classified as a set of shoreline points in the image. The image was geo-referenced by using sophisticated video-processing techniques (Holland et al., 1997). There could be an error in the shoreline detection because of features like water-filled, detached runnel systems or vehicles at the beach. To remove these errors empirical demands on shoreline persistency were used (Aarninkhof et al., 2003).

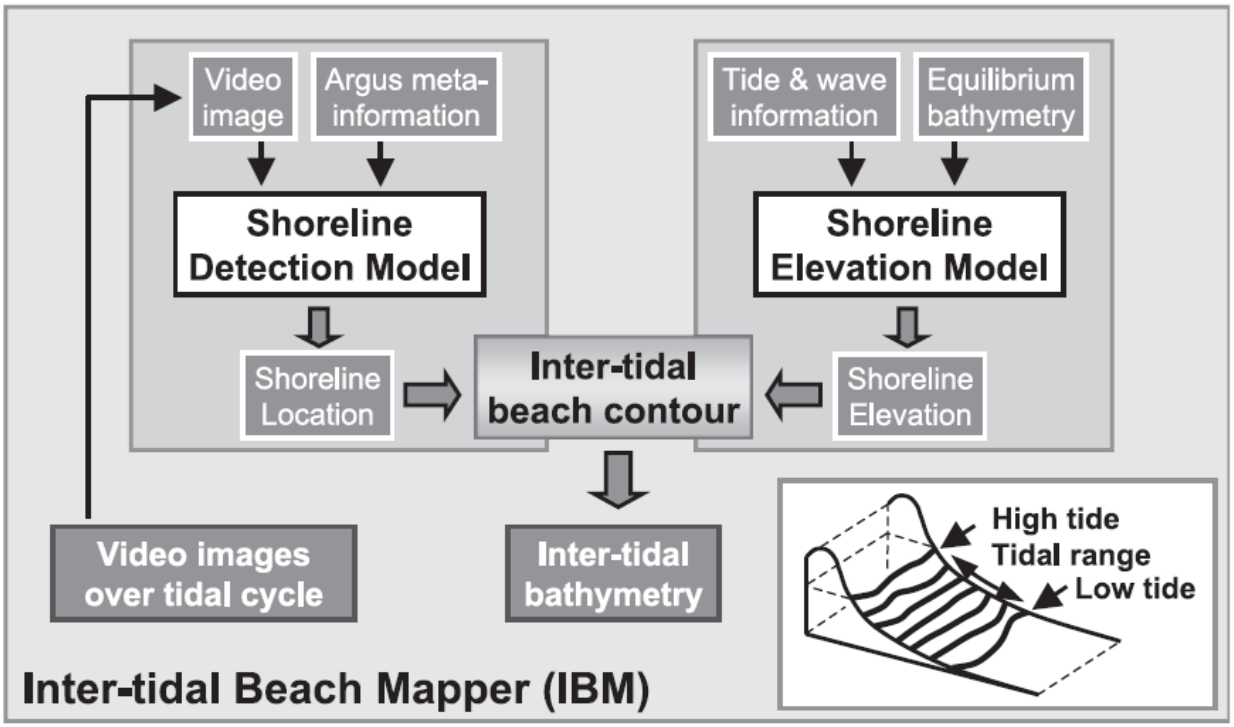

Figure 4.1. Mapping intertidal beach bathymetry from a set of shorelines, derived from time-averaged video observations throughout a tidal cycle. The model consists of two parts: the Shoreline Detection Model and the Shoreline Elevation Model (Aarninkhof et al., 2003).

4.2.2 Shoreline elevation model

The shoreline points were now determined, but to use them for extracting the intertidal beach bathymetry the elevation of the shoreline must be calculated. Several factors were influencing the vertical location of the shoreline points, namely the offshore tidal level, storm surge, breaking induced wave set-up and swash oscillations (Fig. 4.2). The shoreline determined by the shoreline detection model x_{sl} is the shoreline associated with a certain level of swash exceedance. This means x_{sl} was not necessarily located at x_{avg} which is the 10-minute time-averaged shoreline location. The water level elevation z_{sl} of the found shoreline was determined by:

$$z_{sl} = z_0 + \eta_{sl} + K_{osc}\frac{\eta_{osc}}{2} \tag{4.3}$$

where z_0 is the offshore water level induced by the tide- and wind-induced offshore water level without the contribution of gravity waves, η_{sl} represents the wave-breaking induced set-up at the shoreline, η_{osc} is the vertical swash height and K_{osc} is a constant, non-site dependent empirical coefficient that accounts for the level of swash exceedance associated with the beach contour returned from the shoreline detection model (Aarninkhof et al., 2003).

The water level z_0 should be measured close to the coast, preferably within 10 km off the coast, so that the variations in the tide level and storm surge level remained small. The wave set-up η_{sl} was computed with the standard wave decay model of Battjes and Janssen (1998). In this model the roller concept (Svendsen, 1984; Stive and De Vriend, 1994) was incorporated to delay the dissipation of organised energy. An inner surf zone bore model by Aarninkhof and Roelvink (1999) was included to make computations up to zero water depth (Aarninkhof et al., 2003).

The vertical swash height η_{osc} consists of two components: the sea swell swash height R_{ss} (frequency $f > 0.05$ Hz) and the infragravity swash height R_{ig} (frequency $f < 0.05$ Hz). The normalised infragravity

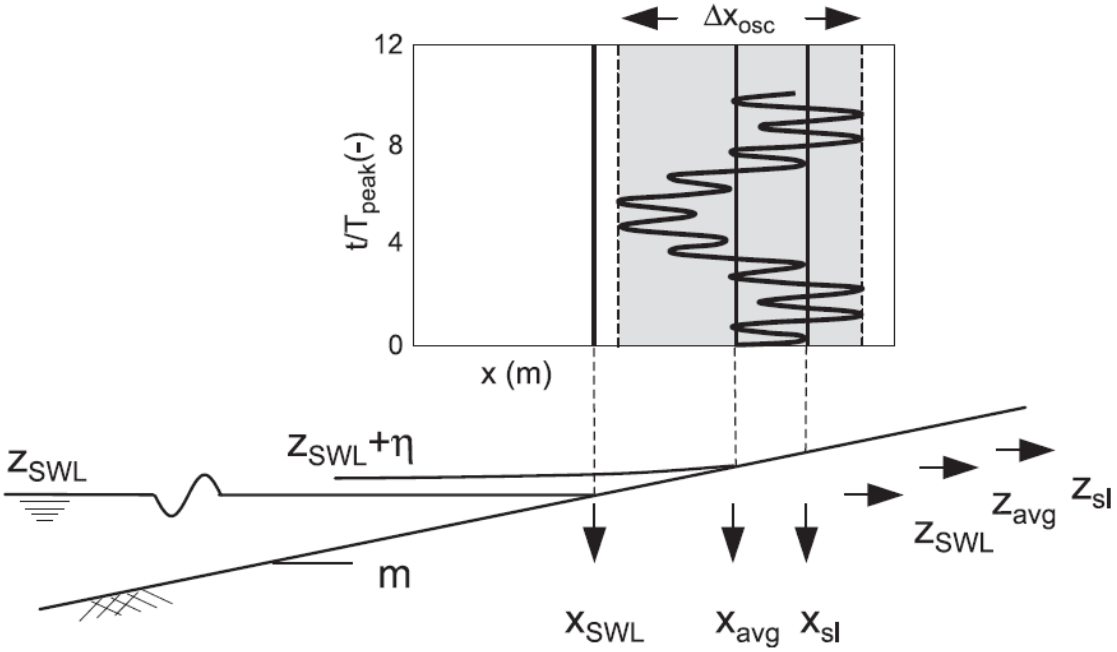

Figure 4.2. Physical processes affecting the instantaneous waterline location. The instantaneous waterline elevation z_{wl} is affected by the offshore water level z_0 outside the surf zone, the breaking induced wave set-up η and an oscillatory component at the time scale of individual waves and wave groups. (Aarninkhof et al., 2003).

swash height R_{ig}/H_0 and the normalised sea swell swash height R_{ss}/H_0 are linearly related to the Iribarren number ξ_0 as:

$$\frac{R_{ig}}{H_0} = 0.53\xi_0 + 0.09 \tag{4.4a}$$

$$\frac{R_{ss}}{H_0} = 0.69\xi_0 - 0.19 \tag{4.4b}$$

where $\xi_0 = \tan(m)/\sqrt{H_0/L_0}$, m is the local foreshore slope and L_0 is the deep-water wave length determined by the peak period T_p. These equations were derived for values of ξ_0 between 0.5 and 3.5 and are generally applicable on various reflective natural beaches (Stockdon et al., 2002). However, on dissipative beaches, like Terschelling (The Netherlands), a significantly larger dependency between R_{ig}/H_0 and ξ_0 was found (Ruessink et al., 1998), namely:

$$\frac{R_{ig}}{H_0} = 2.20\,\xi_0 + 0.02 \tag{4.5}$$

In the IBM it should be possible to map both reflective and dissipative beaches; therefore a relationship suggested by Ruessink et al. (1998) was used, namely:

$$\frac{R_{ig}}{H_0} = 0.65tanh(3.38\xi_0) \tag{4.6}$$

For highly dissipative conditions Eq. 4.6 reduces to Eq. 4.5. On the other hand, for more reflective conditions Eq. 4.6 converges to a value of 0.65. For $0.3 < \xi_o < 0.6$, which lies within the transitional range between reflective and dissipative beaches, there is a lack of measured data. Therefore, it is not established the equation is valid for this range. However, it is the only equation which covers reflective and dissipative beaches and therefore it is used in the shoreline elevation model. To make sure R_{ss}/H_0 is also applicable for highly dissipative conditions Eq. 4.4b has to be adopted. The measured range of ξ_0 by Holman and Sallenger (1985) does not cover highly dissipative conditions ($\xi_0 < 0.275$). As a result, their equation results in a negative R_{ss}/H_0 for those conditions. To resolve this R_{ss}/H_0 is set to 0 for $\xi_0 < 0.275$:

$$\frac{R_{ss}}{H_0} = 0.69\xi_0 - 0.19 \quad for\ \xi_0 > 0.275 \tag{4.7a}$$

$$\frac{R_{ss}}{H_0} = 0 \quad for\ \xi_0 < 0.275 \tag{4.7b}$$

This would mean the contribution of sea swell waves to the vertical swash height would be neglected. However, from the measurements of Ruessink et al. (1998) it can be found that the average ratio of infragravity to total swash height R_{ss}/R was 0.85. This means the contribution of sea swell waves to the vertical swash height on highly dissipative beaches is rather small. The offshore significant wave height H_0 is determined as 4σ where σ represents the standard deviation of the sea surface elevation. The vertical swash height can now be calculated as:

$$\eta_{osc} = \sqrt{R_{ig}^2 + R_{ss}^2} \quad (4.8)$$

where R_{ig} and R_{ss} are obtained from the empirical parameterizations (Eqs. 4.6, 4.7a and 4.7b). The obtained values of z_0, η_{sl} and η_{osc} are then used to estimate z_{sl} (Eq. 4.3) (Aarninkhof et al., 2003).

4.3 Application of IBM

The Intertidal Beach Mapper was a component of the ArgusRuntimeEnvironment. To determine the intertidal beach bathymetry the shoreline was determined for each oblique image available for that day which required the following steps to be taken:

To determine the shoreline a region of interest (ROI) had to be set. The ROI determined the region in which the shoreline was classified. The shape of the ROI influenced whether the shoreline could be classified correctly because the contrast between water and sand had to be clear. When the ROI was set too large the model would for example classify breaking lines above sandbars and patchy wind features on the beach as a part of the shoreline which was of course incorrect (Fig. 4.3B). Also, sometimes the shoreline would be incorrectly mapped as stripy features on the beach (Fig. 4.3B).

The model ran criteria for which method (colour or luminance) was used to determine the shoreline. However, when the model did not choose the right method, the method could be manually set. In general, the colour method tended to give shoreline points which seemed closer to the visible shoreline than the luminance method, but the luminance-method gave a smoother shoreline. Figure 4.3C & 4.3D show the mapped shorelines classified with the colour and luminance methods for the

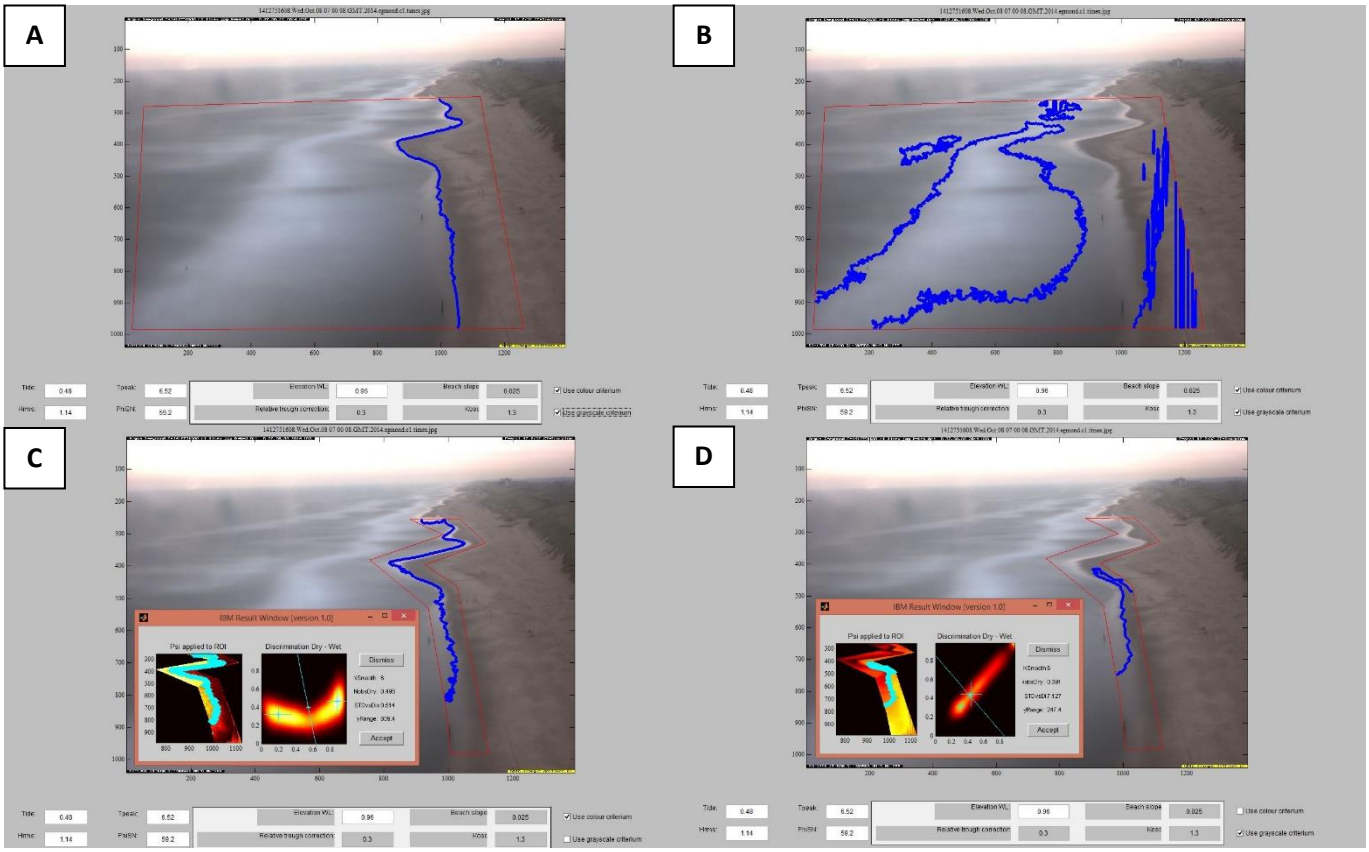

Figure 4.3. A) Correct shoreline classification. B) False shoreline classification because of a large ROI. C) Shoreline classification based on colour criteria. D) Shoreline classification based on grayscale/luminance criteria. The boxes in C and D show the discrimination of dry and wet pixels.

same image and ROI. It can be seen that the two methods could give completely different results. It also shows that one ROI is not always enough to correctly map the shoreline in the whole study area. When the shoreline was incorrect, the other method was used first and then a different ROI was used. When it was not possible to classify the shoreline in one ROI it was attempted to classify the ROI with multiple smaller ROIs. The shoreline determined by the model was manually checked. If the shoreline was classified mostly correct, but had some incorrect points these could be manually removed. Also, shoreline points could be manually added to change incorrect points, map unclassified parts of the beach or link shorelines obtained with multiple ROIs. Figure 4.3A shows a correctly mapped shoreline. To correctly classify this image three ROIs were used. Incorrect shoreline points were removed and the three mapped shorelines in the three ROIs were connected by manually adding shoreline points. Also, the part of the study area located closest to the Argus video tower was not automatically classifiable, so this part of the shoreline was manually mapped.

When it was not possible to determine the shoreline, despite trying different and multiple ROIs, the image was skipped and not included in further analysis. The maximum allowed unclassifiable images per day was dependent on the number of images available on that day, but ranged between one image for days with few images and three images for days with a lot of images. If this limit was exceeded another day was chosen for classification. The importance of the image was also taken into consideration. If for example the low tide image was unclassifiable another day would be selected because this shoreline is used to determine the intertidal beach width.

The number of images classified each day depended on the hours of daylight and the quality of the images. More hours of daylight meant more available images for analysis because the ARGUS system only collected images during daytime. The number of shorelines mapped on a day ranged from 15 to 37. Overall, 96 % of the images of the selected days could be classified. The quality of the images could be negatively influenced by several factors like fog, rain and sun glare. Also, some days were not proper for classification, because the tidal range covered in the images deviated due to high wave conditions. This resulted in a high high water and a high low water which did not include the intertidal bar in the shorelines. Consequently, these data clearly deviated from the other results.

The time between two classification days was one week around the period the SPAW welded to the beach and two weeks in the period further before and after that moment. However, these time periods were not strict because the quality of the images and range of the tide should be taken into consideration. Therefore, the periods between the days used for analysis could differ. For this research only camera 1 was used. The camera was important because camera 2, 3 and 4 only covered a small part of the beach and all the other cameras, including camera 5, were prone to sun glare. This greatly influenced the available images for classification on a day. The shorelines were derived from oblique images instead of plan view images, because the mapped shoreline points on the oblique images were closer to the visible shoreline. The better results are related to the smaller pixel size in the oblique images. However, due to the obliqueness of the images there were less shoreline points classified per meter located further from the camera. Between y = -200 m and y = -300 m there were approximately five shoreline points per meter alongshore while between y = -700 m and y = -800 m there only was 0.4 shoreline point per meter alongshore.

4.4 Extracting dimensions of the intertidal beach

To determine the development of the shoreline, the shorelines collected with the BLIM were smoothed alongshore and subtracted from the actual shoreline. This way the large-scale shape of the shoreline was removed and the effect of the SPAW could be easier determined. The shoreline was smoothed by making use of a Hanning window. The chosen window was 400 pixels which corresponded to 1000 meter alongshore.

From the obtained shorelines several properties of the intertidal beach could be extracted, namely its width, volume and alongshore variability. The intertidal beach width and volume were derived longshore for each y-coordinate. To obtain the intertidal beach width the shoreline locations collected during low and high tide were used:

$$IBW = x_{HT} - x_{LT} \tag{4.9}$$

where IBW is the intertidal beach width, x_{HT} is the cross-shore shoreline location during high tide and x_{LT} is the cross-shore shoreline location during low tide.

However, the part of the tidal range covered each day in the images differed. This was caused by which part of the tide was covered in the images, but also by different wave heights which influenced the wave set-up. Therefore, it was determined to choose one water elevation for low tide and one water elevation for high tide so the tidal range was approximately equal. The low tidal level was set at -0.25 m and the high tidal level was set at 1.41 m for the analysis of the volume. These values were the average water elevations of all low tides and high tides classified. For the analysis of the intertidal beach width the low tidal level was set at -0.18 m and the high tidal level was set at 0.99 m. This tidal range for the volume analysis was larger, because the loess interpolation also interpolated areas which were lower and higher than the lowest and highest mapped shoreline. These values were chosen to include as much classified days as possible without losing important information like intertidal bars.

For the determination of the intertidal beach volume a bathymetry of the intertidal area was required. With the help of a quadratic loess interpolation method (Plant et al., 2002) a 1 m by 1 m bathymetry was computed from the shorelines collected for each day. A quadratic loess interpolation method was used, because it includes morphological length scales in its interpolation. The cross-shore length scale L_x used was 20 m and the alongshore length scale L_y used was 150 m. These scales were based on the lowest interpolation error (0.038 m), the lowest RMSE when compared to the validation data (0.17 m) and the presence of gaps in the bathymetry.

From the computed bathymetry, all elevations above the high water level and below the low water level were removed, so only the intertidal area remained. From this bathymetry the volume of the intertidal area could be determined:

$$V = \sum_{i=1}^{n_x-1} \left(z_i - \frac{1}{2}(z_i - z_{i+1}) - z_{LT} \right) * (x_i - x_{i+1}) \tag{4.10}$$

where V represents volume of the intertidal beach, n_x represents the number of cross-shore beach elevations, z represents the beach elevation, x represents the cross-shore location, and z_{LT} represents the shoreline elevation during low tide. The total volume of the intertidal beach in the

study area was calculated as the sum of each alongshore volume. The total volume was also calculated for a range of elevations to determine the vertical distribution of the intertidal beach volume.

To determine the alongshore variation in the shoreline location the standard deviation was calculated alongshore:

$$Sd_{sh} = \sqrt{\frac{\sum_{i=1}^{n_y}(x_i - x_{mean})^2}{n_y - 1}} \tag{4.11}$$

where Sd_{sh} is a measure of the alongshore variability of the shoreline over a range of y-coordinates and n_y is the range of y-coordinates over which the alongshore variability will be calculated. This was done for the shorelines of the whole Egmond area (4000 m) and in the study area (600 m) obtained with the BLIM, and for the shorelines obtained with the IBM.

4.5 Model uncertainties

4.5.1 IBM uncertainties

The shoreline points classified by the IBM can have vertical and horizontal errors. In this study the mapped shorelines were not validated against GPS-surveyed shoreline. However, Aarninkhof et al. (2003) did validate the vertical and horizontal location of the shoreline points mapped by the IBM for the Egmond coast in their study. They found that the mean absolute vertical offset was less than 15 cm along more than 85% of the 2-km-long stretch of beach they mapped. In general, the further away the shoreline points were located from the Argus tower the larger the model deviations were. An absolute vertical offset of 15 cm corresponds to a mean horizontal offset of 6 m. The mean vertical offset for the whole area was -8.5 cm which indicated that there was a landward offset of the shoreline points obtained by the IBM. The standard deviation of the vertical deviations was 17.4 cm. However, this was largely compensated by the mean elevation induced offset of 7.8 cm with a standard deviation of 12.6 cm (Aarninkhof et al., 2003). The poorer classification of shoreline points located further away can be explained by the decrease of pixel resolution in the far field. It should be noted that the validation data also showed an error because the instantaneous location of the shoreline is affected by swash motion (Aarninkhof et al., 2003). When the shoreline points were validated against surveyed bathymetric data at Egmond an RMSE of 0.17 m was found (Plant et al., 2007).

For some images the contrast between water and sand in the image would be different over the image and therefore the model would not be able to classify the whole shoreline. By using multiple ROIs to cover the study area these shorelines could be better classified. Therefore the shoreline points mapped for this study were likely to be more accurate than the shoreline points mapped by Aarninkhof et al. (2003). On the other hand, sometimes parts of the image had to be manually classified. For some images the shoreline was hard to distinguish, but still mapped. This could result in a large offset compared to the real shoreline location which is of O(0.1 – 1 m).

To make a fair comparison between the intertidal beach widths of the study area of each day, the tidal range was set between -0.18 m and 0.99 m. However, images were only collected every half an hour and therefore did not correspond with the chosen low water and high water elevation.

Therefore, days were chosen where the timex images did cover low water and high water elevations which did not vary more than 0.05 m from the chosen low tide and high tide elevations. However, this could still result in a large difference in tidal range which could affect the intertidal beach widths which is of O(1-10 m).

4.5.2 Interpolation

The shoreline points were interpolated into a 1 m by 1 m bathymetry with a loess interpolation (Plant et al., 2002). The cross-shore length scale L_x and alongshore length scale L_y chosen for the interpolation were based on the lowest RMSE, interpolation error and the presence of gaps in the interpolated bathymetry. Eventually, L_x = 20 m L_y = 150 m were chosen. These scales showed the lowest RMSE (0.17 m) and had an acceptable interpolation error (0.038 m). The interpolation errors were lowest for small length scales, but often had a high RMSE and gaps in the bathymetry which made them unreliable.

There were some factors which may have affected the interpolation of the shoreline data. First, the number of shorelines classified differed per day. During the summer months daylight lasted long, therefore a lot of timex images were present for these days, but during winter months the days became shorter and the number of timex images available for classification became less. For example, on 15 July 2014 36 shorelines were mapped within a time span of 03:00 GMT till 20:30 GMT. On the contratry, on 5 December 2014 only 15 shorelines were mapped within a time span of 09:00 GMT till 16:00 GMT. Where it would be expected that more shorelines contribute to a more reliable interpolation this was not seen in the interpolation errors (Fig. 4.4A). It even seemed the interpolation errors were lower when less shorelines were classified. A possible explanation could be

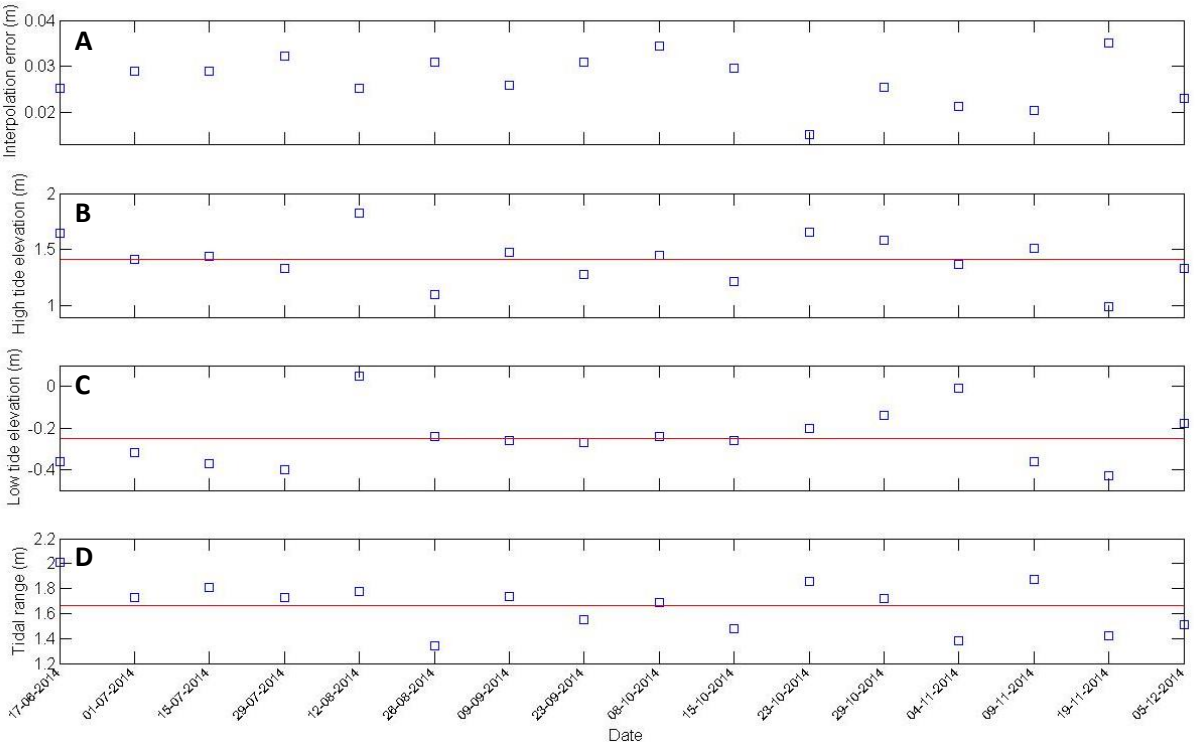

Figure 4.4. A) The interpolation error of the interpolated intertidal beach bathymetry (-0.25 m – 1.41 m). B) The maximum water level captured in the Argus images of that day (m). The red line is the chosen high water level (1.41 m). C) The minimum water level captured in the Argus images of that day (m). The red line is the chosen low water level (-0.25 m). D) The tidal range captured in the Argus images of that day (m). The red line is the chosen tidal range (1.66 m).

that on shorter days the timex images only cover one tidal cycle and therefore are consistent with each other. During longer days the timex images would cover two tidal cycles and more variation in a day would be present**.** Second, the manually added shoreline points may have affected the interpolation errors. Where the IBM classified the shoreline points with a similar distance between each point, this was not the case for the manually added points. The distance between the manually added points varied and was coarser or finer than the other shoreline points. The interpolation used shoreline points in the specified alongshore and cross-shore range to determine an elevation point for the bathymetry. This would mean this point was then affected more/less by the manually added shoreline points than by the automatically generated shoreline points. Third, for the interpolation no equally-spaced grid of shoreline points was used. The locations of the shoreline points were dependent on the shorelines covered in the timex images. The middle part of the intertidal beach was less covered than the upper and lower part of the intertidal beach because the tide rises and falls fast in this area of the intertidal beach. Also, less shoreline points were classified per distance alongshore further away from the camera because the area covered in a pixel increased further away from the camera. This affected the number of shoreline points used for the interpolation of each bathymetry point. Fourth, the high tide elevation, low tide elevation and the tidal range covered in the timex images for each day differed. On 12 August 2014, 26 August 2014, 4 November 2014 and 19 November 2014 the computed volumes really differed from what was expected. This can be explained when looked at the high tide elevation, low tide elevation and tidal range covered on these days (Fig. 4.4B, 4.4C & 4.4D). On 12 August 2014 the high tide elevation (1.83 m) and low tide elevation (0.05 m) were higher than on any other day which was caused by large wave heights (> 2 m) on this day. Due to this a large part of the lower intertidal zone was not covered in the mapped shorelines. The lower part of the intertidal zone was also not covered on 4 November 2014. This probably resulted in an overestimation of the volume on these days. On 26 August 2014 the high tide (1.10 m) and tidal range (1.34 m) covered on this day were low. The reason for this is unknown, but in this case this also resulted in an overestimation of the volume. However, the interpolation errors of these days were similar compared to other days which indicated the problem was probably related to the IBM. On 19 November 2014 the wave conditions were extremely low (~0.6 m) which resulted in a low high tide elevation (0.99 m), a low low tide elevation (-0.43 m) and a low tidal range (1.42 m). On this day the interpolation error (0.033 m) was high compared to other days in this period. This resulted in a large underestimation of the volume. When the shorelines did not cover the whole tidal range the interpolation tended to give incorrect values at the edges of the bathymetry. At the seaward side of the bathymetry the bathymetry sometimes increased again which was incorrect because this was located seaward of the low tide line. In addition, sometimes an incorrect maximum was reached in the upper part of the bathymetry and the bathymetry decreased landward of this maximum. Both these effects caused an incorrect increase of the volume.

4.6 Validation

To determine how reliable the interpolated bathymetries were, the bathymetry of 8 October 2014 was compared to ground truth data obtained with a MLS. The ground truth data were collected on 10 October 2014. These data were compared to the interpolated bathymetry of 8 October 2014 because this was the closest day which could be properly classified. To compare the validation data to the obtained bathymetry, the data were reshaped to the extents of the bathymetry obtained by the interpolation of the mapped shorelines. Then the heights of each pixel were subtracted to determine the difference:

$$\Delta z(x,y) = z_{val}(x,y) - z(x,y) \quad (4.12)$$

where Δz is the difference between the validation data and the interpolated bathymetry, z_{val} is the validation height, z is the interpolated beach elevation, x represents the cross-shore location and y represents the alongshore location.

The interpolated bathymetry and the validation bathymetry are shown in Figure 4.5A & 4.5B, respectively. It can be seen that the lower part of the intertidal area (< 0.2 m) covered a larger area for the interpolated data than for the validation data. This part of the intertidal beach was not covered by the MLS. Besides that, the shape of the intertidal zone was similar. Only the direction in which the seaward protrusion was pointing was different. Figure 4.5D shows the difference between the interpolated bathymetry and the validation bathymetry. The pixels where only one of the bathymetries was present were not included. The mean difference between the two bathymetries was -0.022 m with a standard deviation of 0.17 m. The RMSE was 0.17 m. It should be noted this only considered the area where both datasets were present. It seemed the landward edges of the area show a clear underestimation of the real elevation which could be related to the large interpolation errors (Fig. 4.5C). However, the maximum interpolation error was not lowered because the upper part of the intertidal beach would then be excluded. Also, a large overestimation was present on either side of the seaward protrusion of the shoreline while the centre of the protrusion showed an underestimation. The validation volume calculated was 19,977 m³ and the interpolated volume was 23,317 m³. The negative mean difference seemed incorrect because the total interpolated volume was larger, however the difference could only be determined for the locations the validation and interpolation bathymetry both have data. As can be seen in Figure 4.5, the

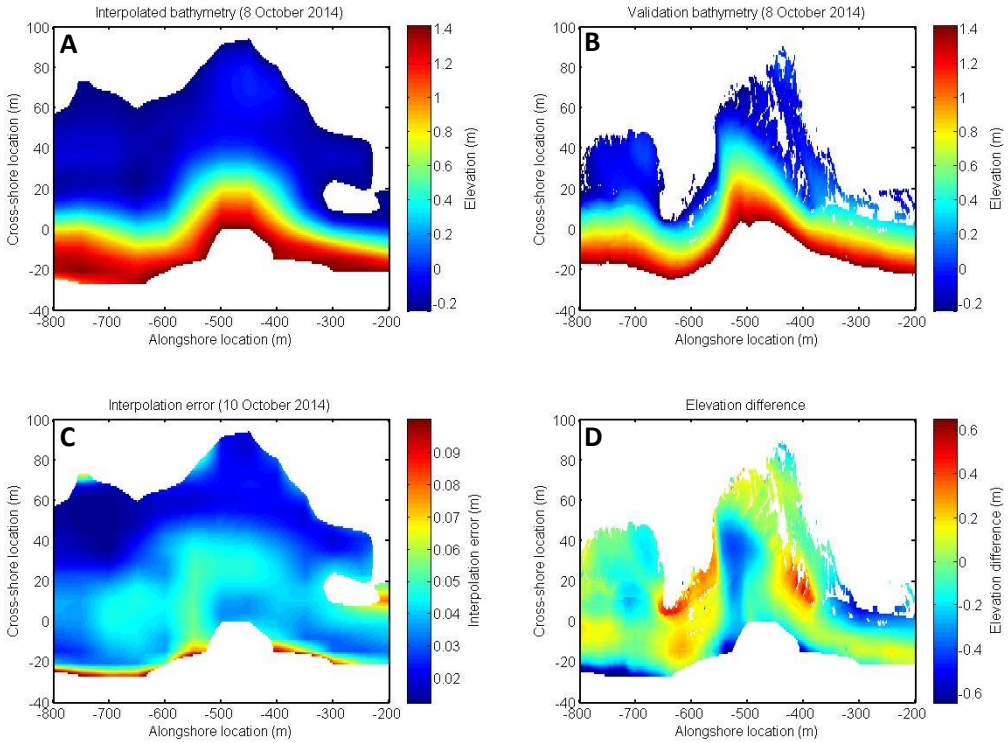

Figure 4.5. A) The interpolated bathymetry of 8 October 2014. B) The validation bathymetry of 10 October 2014 obtained with the MLS. C) The interpolation error of the interpolated bathymetry of 8 October 2014. D) The difference between the interpolated bathymetry and the validation bathymetry. Positive means the interpolated elevation is overestimated and negative means the interpolated elevation is underestimated.

validation data did not cover a large part of the lower intertidal zone and a part of the upper intertidal zone which was included in the total interpolated volume. Therefore, the volumes were determined for the locations both bathymetries covered. The validation volume was 19,552 m^3 while the interpolated volume was indeed smaller, namely 16,301 m^3.

It should be noted that on other days the difference between the interpolated data and the real beach elevations could be completely different because the quality of the mapped shorelines and the computed elevations could really differ for each day. An indicator for the reliability of the mapped shorelines is the deviation of the high tide elevation, low tide elevation and tidal range from the red lines in Figure 4.4. The days which were considered unreliable all show deviation from the red line in one or more of these characteristics. A low interpolation error does not directly mean the bathymetry is reliable. An example of this is 12 August 2014 where the interpolation error is relatively low. On this day the mapped shorelines were probably unreliable and so the interpolated bathymetry. Still, the results from the IBM are considered reliable enough to study the impact of SPAWs on the intertidal beach (-0.02 ± 0.17 m). However, when looking at the results it should be taken into consideration that there are uncertainties.

Chapter 5 Results

5.1 Observed SPAW event

At Egmond, 15 SPAW events emerged from the inner bar which migrated to the coast in 2014. Of these SPAW events only 8 events eventually merged with the shoreline (Price et al., 2017). The alongshore locations and periods of the SPAW events that merged with the shoreline are shown in Table 5.1. The mean shoreline location between 1 January 2014 and 25 September 2015 is shown in Figure 5.1. It can be seen that the mean shoreline was mainly located between 80 m and 90 m. However, between y = -1300 m and y = 500 m the shoreline was located more shoreward, around 70 m. In this embayment at approximately y = -450 m the shoreline extended approximately 5 m more seaward. The location of this bulge corresponded to the occurrence of the fourth SPAW event (Table 5.1). In Figure 5.2 the deviation from the smoothed shoreline is shown for each day. The seaward protrusion of the shoreline occurring at y = -450 m was present during the whole period. Furthermore, it reveals that the alongshore location of the edges of the embayment (around y = -1200 m and y = 200 m) showed a positive deviation from the smoothed shoreline which roughly corresponded with SPAW events 2 and 3 at the northern border and SPAW events 5, 6 and 7 at the southern border. A change in the deviation from the smoothed shoreline seemed absent for the eight SPAW event. For SPAW event 1 a small change could be seen, however this was too vague to directly link to an effect of the SPAW. The morphology of the shoreline in 2015 could also be affected by SPAWs emerging in 2015, but unfortunately these data were not available. In the rest of this study the focus will be on the impact of the fourth SPAW event on the intertidal beach and the shoreline.

Table 5.1. Alongshore locations and period of SPAW events in 2014. (Van Kuik, 2016).

#	Alongshore location SPAW (m)	Period (months)
1	-1500	Oct – Nov
2	-1200	Oct – Nov
3	-1100	Apr – Aug
4	-450	Oct - Nov
5	175	Sep – Oct
6	225	Jul – Aug
7	375	Nov - Dec
8	1800	Apr - May

The SPAW event analysed was located at y = -450 m. Before the SPAW emerged from the sandbar there was already an out-of-phase coupling between the inner bar and the shoreline (Fig. 5.4A). The horn of the highly 3D crescentic inner bar was directed in onshore direction at the same location where the SPAW would eventually develop. The shoreline at this location already showed a seaward protrusion before the SPAW even developed. On 9 July 2014 there were high wave conditions (3.5 - 4 m) (Fig. 5.3A&B) and the horn was split (Fig. 5.4A). The SPAW could now be seen as a separate

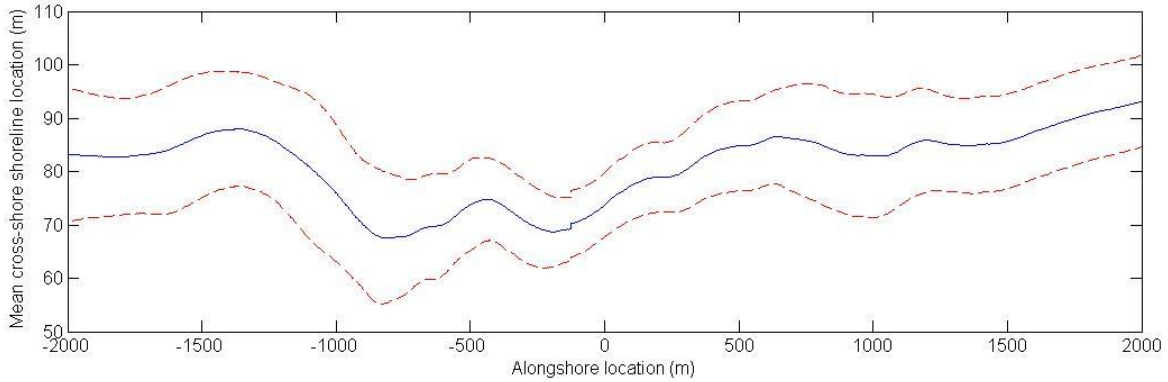

Figure 5.1. The blue solid line represents the mean cross-shore bar location between 1 January 2014 and 25 September 2015. A higher value means the shoreline is located more seaward. The red dashed line represents one standard deviation from the mean.

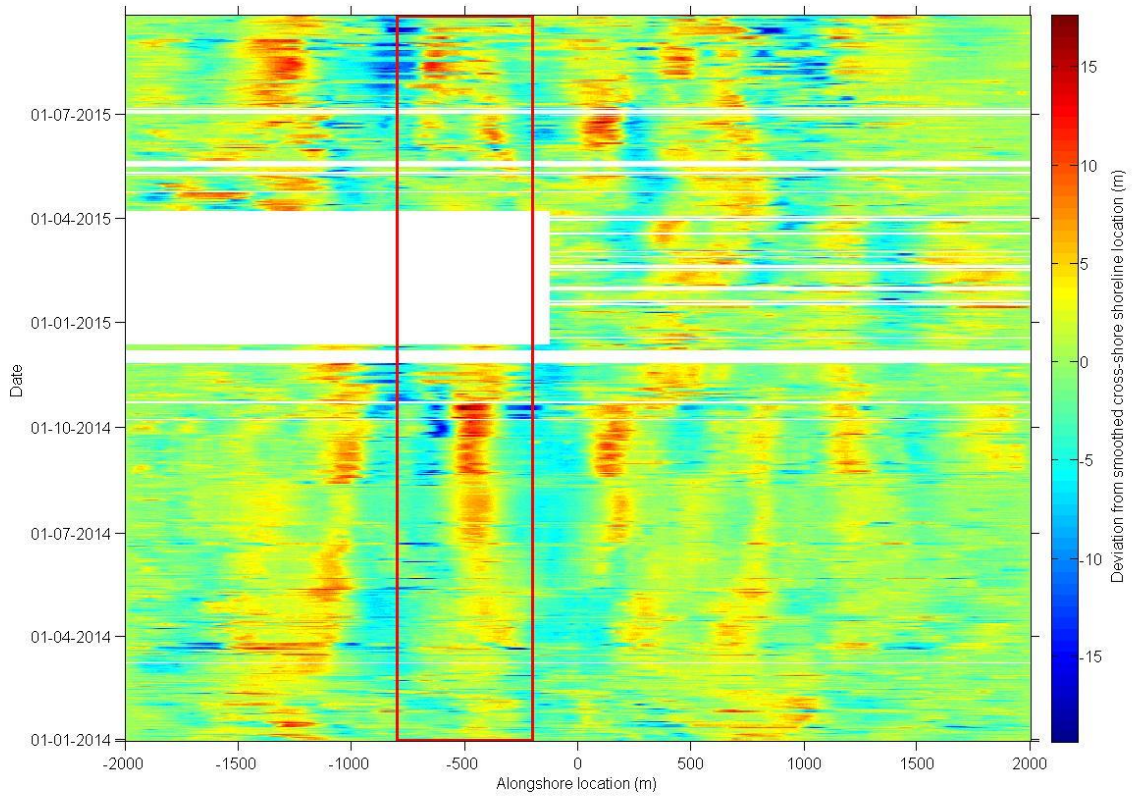

Figure 5.2. Time stack showing the deviation of the smoothed shorelines from the actual shoreline over time and alongshore location. Red means the actual shoreline was located more seaward than the smoothed shoreline. The red box indicates the study area in which the SPAW event was analysed. The alongshore location will be named y.

feature from the inner bar. Also, at approximately y = 200 m a SPAW separated from the inner bar. According to Van Kuik (2016) the SPAW event emerged end September/begin October 2014 and merged with the shoreline around begin November. However, when looked at the plan view images (Fig. 5.4) the SPAW event seemed to emerge earlier. Around 11 July 2014 the SPAW could be identified as a separate feature from the inner bar on the plan view images for the first time (Fig. 5.4A). However, the SPAW still showed some connection to the bar. Prior to its formation the SPAW was a part of the horn of the inner sandbar. On the plan views with high waves only the horn was clearly visible. The mechanism for SPAW formation was bar splitting and seemed to be related to high wave conditions (3.5 – 4 m) (Fig. 5.3A & B) and highly oblique waves from the north (~80°) (Fig. 5.3D & E). The SPAW migrated to the shoreline and can be last seen as an individual feature on the plan view image at 10 October 2014 (Fig. 5.4B). In general, the migration speed of the SPAW was low. Only in the last days, when the SPAW was fully separated from beach, the migration speed increased. However, the exact migration speed is unknown because no data about the position of the SPAW were available. The wave heights just before (2-3 m) and during (2-6 m) the period the SPAW merged to the shoreline were considerably higher than during calm conditions (~1 m) (Fig 5.3A & C). The extremely high wave conditions (up to 6 m) around 21 October occurred after the SPAW connected with the shoreline, but it is not sure whether the SPAW already completely merged with the shoreline. Lastly, it should be noted that the dates of SPAW emergence and SPAW merging are not exact, because it was hard to determine when a SPAW was a separate feature. Therefore, the period of emergence will be taken between 29 June 2014 and 19 July 2014 and the period of merging with the shoreline between 2 October 2014 and 27 October 2014. The SPAW was at least 175 meters long and 20 meters wide based on the foam patch in the plan view of 9 October 2014.

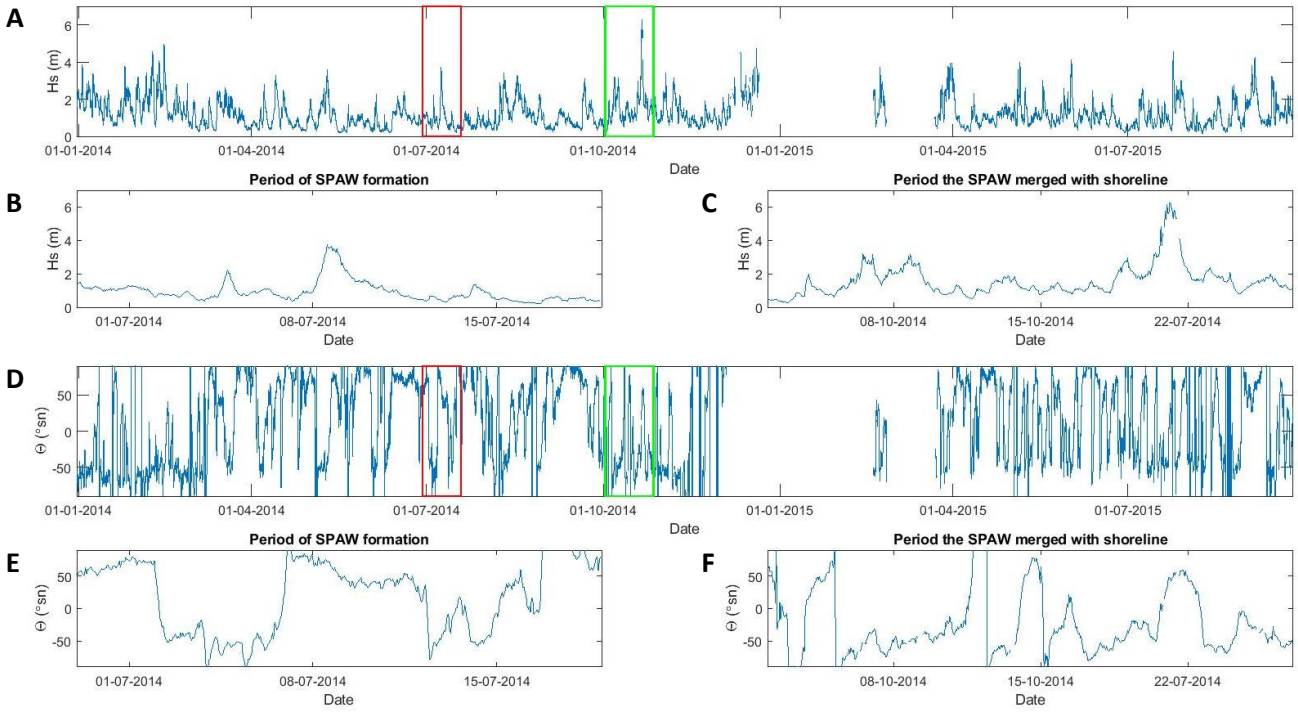

Figure 5.3. A) Wave height H_s (m) during the whole study period. D) Angle of wave incidence θ (°) relative to shore normal during the whole study period. The red box indicates the period of SPAW formation (B & E) and the green box indicates the period the SPAW merged with shoreline (C & F). Data retrieved from http://live.waterbase.nl.

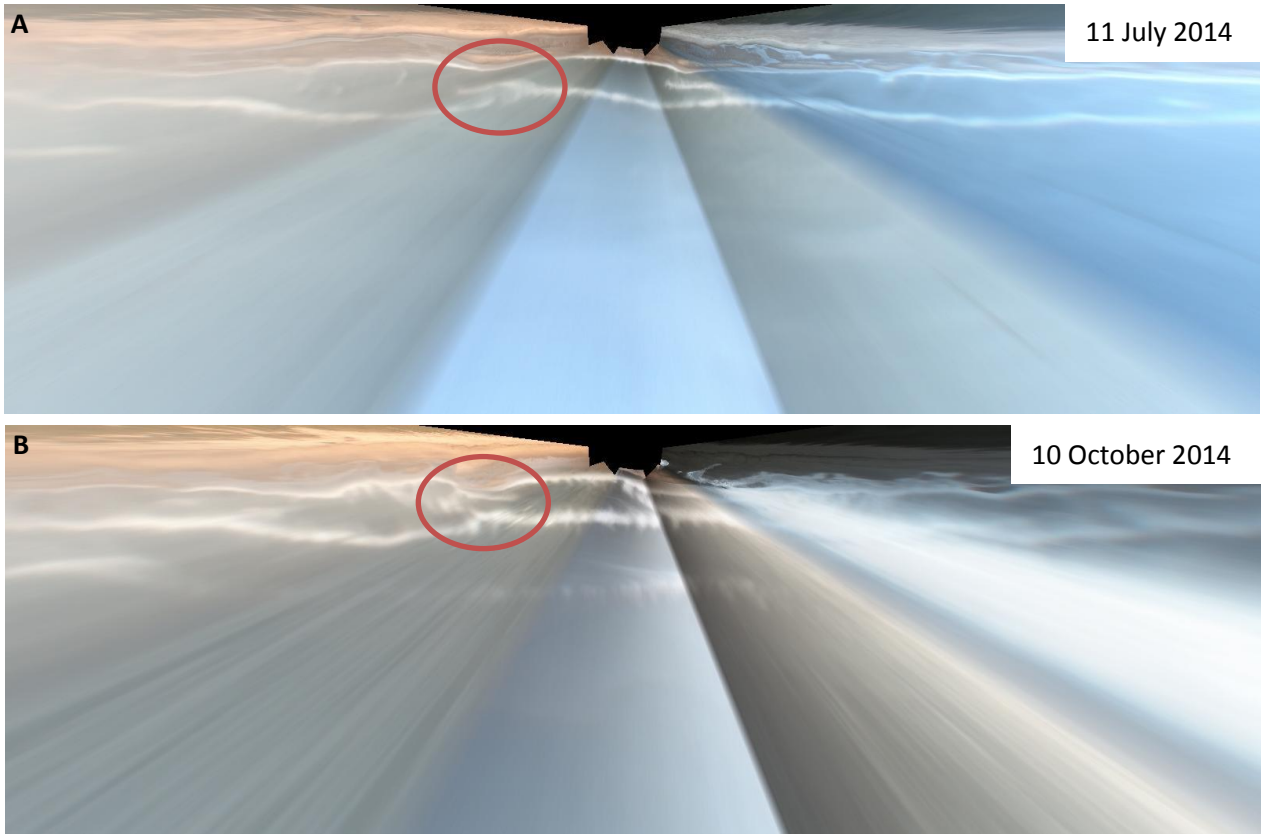

Figure 5.4. A) planview image of 11 July 2014. This is one of the first days the SPAW can be seen as a separate feature from the inner bar. B) planview image of 10 October 2014. This is one of the last days the SPAW can be seen as a separate feature from the shoreline.

5.2 Alongshore-averaged shoreline position

5.2.1 Shoreline position

In January 2014, the deviation from the smoothed shoreline in the embayment showed little variation alongshore (Fig. 5.2). Around begin March 2014 the seaward protrusion narrowed and became more distinct. Especially the areas next to the seaward protrusion seemed to deviate more from the smoothed shoreline, meaning the shoreline moved more landward in these areas (blue areas). Around mid-May 2014, the narrowing stopped and the width of the seaward protrusion seemed to be stable until end October 2014. On the other hand, the deviation from the smoothed shoreline increased positively (darker red) for the seaward protrusion and negatively for the adjacent areas (darker blue). After October 2014 the deviation from the mean shoreline location decreased again at y = -450 m. Unfortunately, it was hard to tell what happened after this decrease because shoreline data were missing in this period. In the period after the data gap it can be seen that the morphology of the shoreline changed. Up to approximately mid-May 2015 the deviation from the smoothed shoreline became smaller and no clear seaward protrusion was visible anymore.

To determine the impact of the SPAW on the shoreline position, the alongshore-averaged cross-shore shoreline position in the study area was compared to the alongshore-averaged cross-shore shoreline position of the whole area. The alongshore-averaged cross-shore shoreline location is shown in Figure 5.5A. The shorelines collected with the BLIM tool were the low tide shorelines and

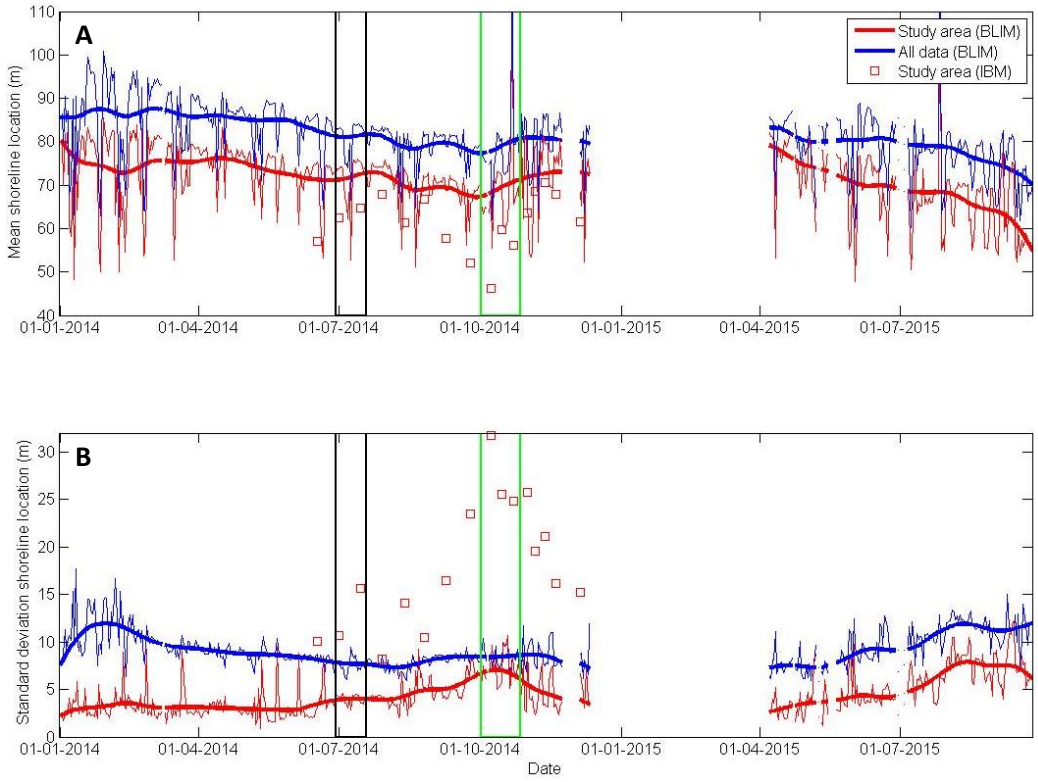

Figure 5.5. A) The mean cross-shore shoreline location for each day of the study period for the whole Egmond area (blue line) and the study area (red line). B) The standard deviation of the cross-shore shoreline location for each day of the study period for the whole Egmond area (blue line) and the study area (red line). The solid lines represent data collected with the BLIM tool and the red squares represent data obtained with the IBM. The thin lines are the real data collected with the BLIM tool, while the thick lines show the same data but smoothed over 50 days with a Hanning window. The thick lines show the general trend of the mean and standard deviation. The outlying values are mostly caused by high wave conditions which cause an incorrect classification of the shoreline. The black box indicates the period of SPAW formation and the green box indicates the period the SPAW welded with the shoreline.

therefore they are only compared to the low tide lines obtained with the IBM. The high tide shorelines obtained with the IBM are discussed in section 5.3.1. Along the Egmond coast a gradual decrease in the mean position of the shoreline was seen from approximately 90 m to 75 m. However, begin October 2014 this trend was disturbed. In the period hereafter, the mean cross-shore shoreline position increased. It is not known until when and how far because the shoreline data between 11 December 2014 and 7 April 2015 was absent. After 7 April 2015 the shoreline data were available again. The mean shoreline position on this day showed it increased to at least 85 m. After the data gap a gradual decrease could be seen again to approximately 70 m on 1 October 2015 which was the last day of the study period. The mean cross-shore shoreline position in the study area showed a similar trend, but was initially located more shoreward (~80 m). However, the difference between the mean shoreline position for the whole Egmond coast and the study area varied over time. The mean shoreline location in the study area was located more landward and until begin October 2014 the difference in shoreline position was approximately 10 m (Fig. 5.5A). In the following period this difference decreased because the mean cross-shore shoreline position showed a larger increase in the study area than in the whole area. After the data gap, it can be seen that this difference was even smaller (~5 m on 7 April 2015). In the remaining days the difference got larger again to around the same difference as in the first period. It should be noted that the mean cross-shore shoreline position for the whole area and the study area were linked because the study area was a part of the Egmond coast. The mean cross-shore shoreline location data obtained with the IBM showed a similar trend as the mean cross-shore shoreline location data obtained with the BLIM tool. Only the magnitude of the changes was higher. During the period of SPAW emergence the mean cross-shore shoreline location did show a small increase. However, this increase was only 10 m and lasted for a short period. On the other hand, the increase of the mean shoreline position during the period the SPAW merged with the shoreline was considerably larger (~25 m). The maximum mean cross-shore shoreline position after this period was not known because of missing data.

5.2.2 Alongshore variability

In Figure 5.5B the standard deviation of the cross-shore shoreline position is shown. In the whole Egmond area the standard deviation of the shoreline position was in the range of 7 to 12 m for the period between approximately mid-February 2014 and early December 2014. After the large data gap, the standard deviation showed an increase from approximately 7 m to 12 m. The standard deviation in the study area was smaller and showed another trend. The standard deviation varied between 3 m and 5 m until mid-June 2014. After this period the standard deviation showed a considerable increase to approximately 8 m. This peak was reached in mid-October 2014. Hereafter, the standard deviation decreased again to at least 2.6 m on 7 April 2015. This change in standard deviation was not seen in the whole Egmond area. After 7 April 2015 the standard deviation showed a similar increase as could be seen for the whole area to approximately 8 m. The standard deviations obtained by the IBM were much higher, but the increase in standard deviation between mid-June 2014 and mid-October 2014 (from approximately 10 m to 30 m) and the decrease afterwards (from approximately 30 m to at least 15 m) could also be seen for these data. The increase in standard deviation seemed to start around the period of SPAW formation. Clearer is the fact that the peak of the standard deviation corresponded with the period in which the SPAW merged with the beach.

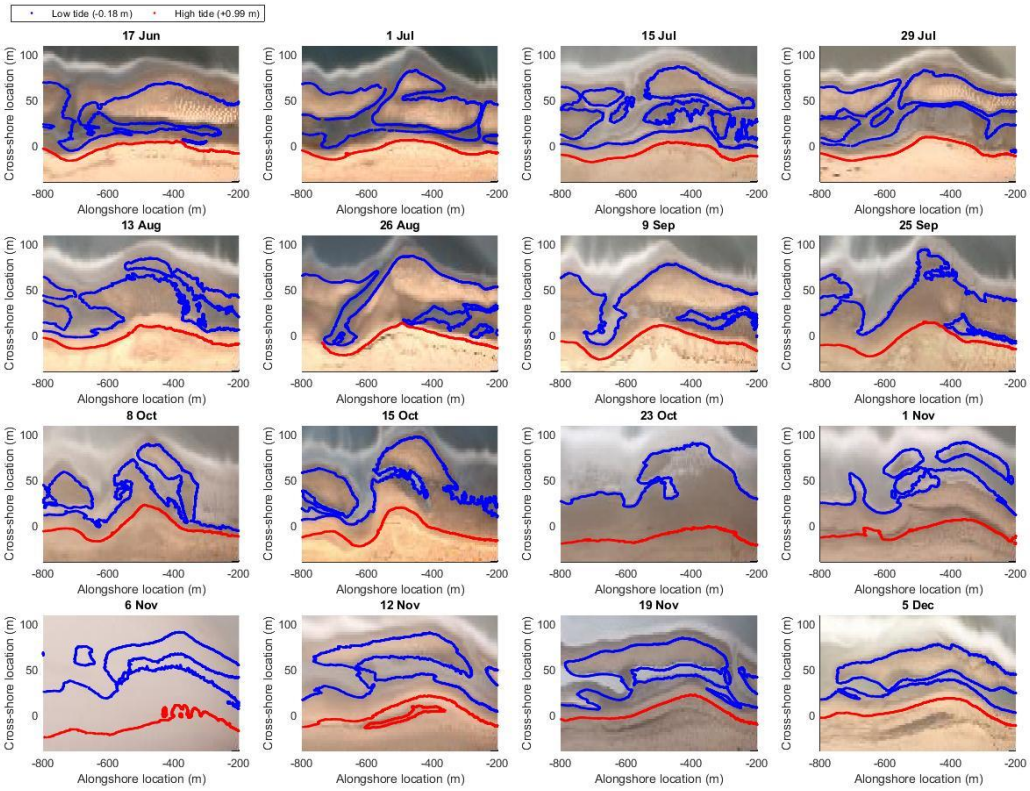

Figure 5.6. The blue lines indicate the low water line (-0.18 m) and the red lines represent the high water line (+0.99 m) collected with the IBM. These were not the actual low and high tide shorelines, but to make a good comparison one value was chosen which was available for all selected days. Therefore, the mapped low tide lines do not always coincide with the actual shorelines in the image. The shoreline elevations differed ± 0.05 m from the chosen values. The cross-shore location will be named x and the alongshore location will be named y.

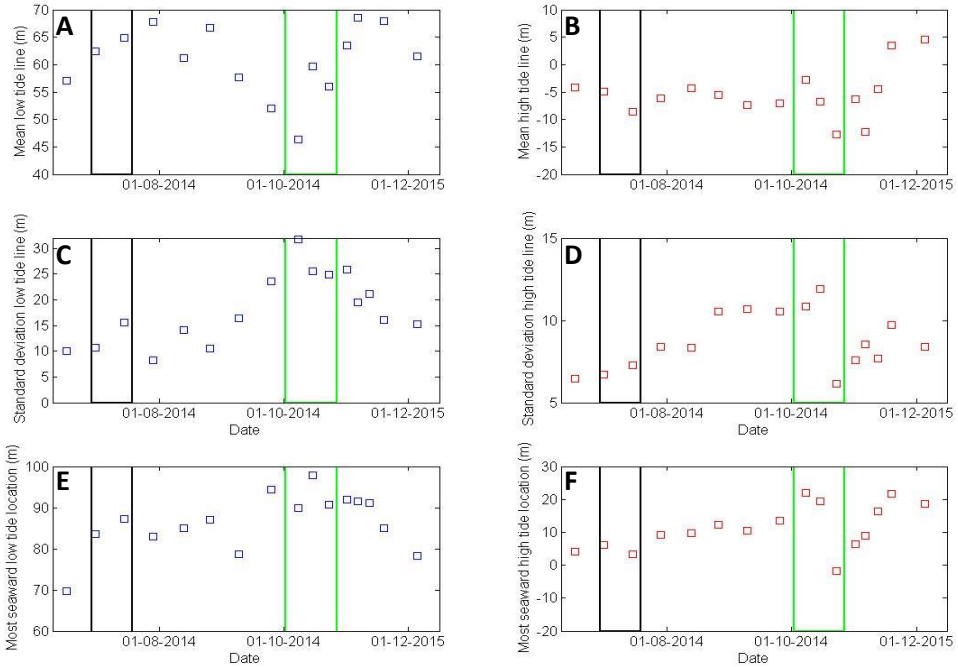

Figure 5.7. Mean (top row), standard deviation (middle row) and maximum (bottom row) of the low (-0.18 m) (left panels) and high tide (+0.99 m) (right panels) line collected with the IBM. The colours of the data correspond to the colours of the shorelines shown in Figure 5.6. The black box indicates the period of SPAW formation and the green box indicates the period the SPAW welded to the shoreline. The data in panel A & C are also displayed in Figure 5.5.

5.3 Intertidal beach morphology

Figure 5.6 shows all low (-0.18 m) and high (+0.99 m) tide lines collected with the IBM. On 17 June 2014 the SPAW was not yet a separate feature; however there was an out-of-phase coupling between the inner bar and the shoreline (Fig. 5.4). Therefore, around y = -450 m the low and high tide line already protruded more seaward. Furthermore, it can be seen that around x = 25 m there was a depression with a connection to the sea between y = -700 m and y = -600 m (Fig. 5.6). During high tide the intertidal bar was submerged. The depression between the upper intertidal beach and the intertidal bar was completely submerged in longshore direction until 29 July 2014. After that the depression was not submerged between approximately y = -550 m and y = -400 m during high tide. On 23 October 2014 the intertidal bar was merged with the upper intertidal area. In the same period the seaward protrusion at y = -450 m became more pronounced. When looking at the seaward protrusion itself it can be seen that on 13 August 2014, 25 September 2014, 8 October 2014, 15 October 2014 and 23 October 2014 a part of its centre was located below low tide. After the period of SPAW merging (early/mid-October 2014) the seaward protrusion seemed to disperse alongshore. As a result, a new intertidal bar formed in November/December.

5.3.1 Intertidal beach width

The development of the low tide line is already discussed in relation to the shoreline location in section 5.2, but with the IBM also the high tide line was mapped. The mean, standard deviation and maximum of the high and low tide shoreline positions are plotted in Figure 5.7. The mean high tide shoreline positions showed a similar increase as the mean low tide shoreline positions after the SPAW welded to the beach. However, in the period before the mean high tide shoreline position remained stable between approximately -10 m and -4 m where the mean low tide shoreline position clearly showed a decrease from approximately 70 m to 45 m. In the period before the SPAW welded

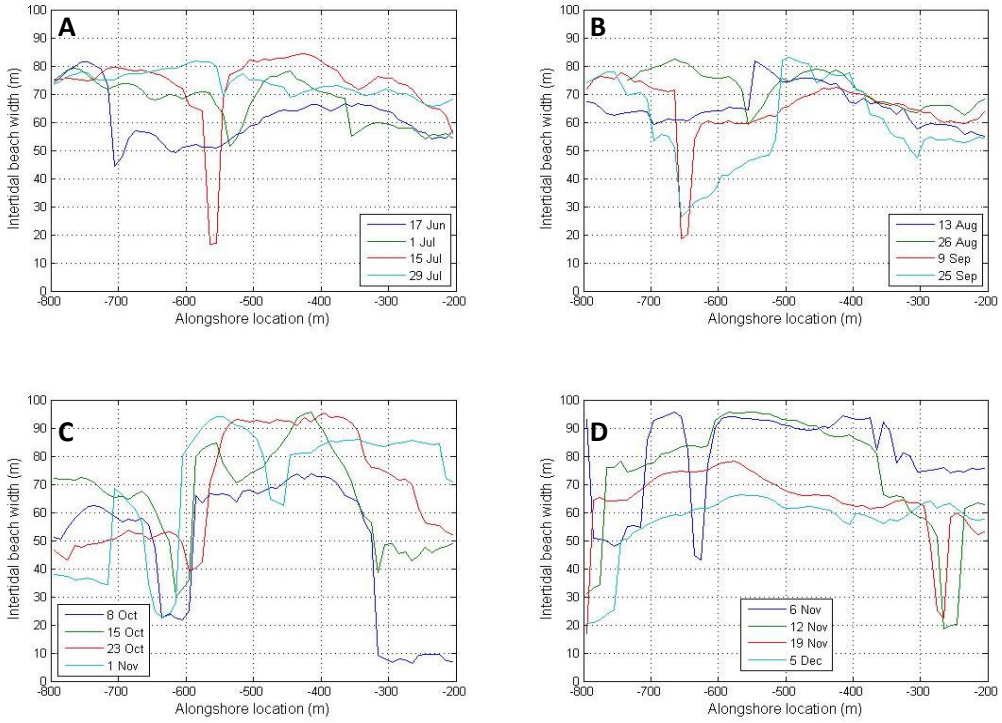

Figure 5.8. The intertidal beach width alongshore (m) over time collected with the IBM (in 2014). A) IBW of 17 June, 1 July, 15 July and 29 July. This period included the period of SPAW emergence. B) IBW of 13 August, 26 August, 9 September and 25 September. This period was between SPAW emergence and SPAW welding. C) IBW of 8 October, 15 October, 23 October and 1 November. This period included the period of SPAW welding. D) IBW of 6 November, 12 November, 19 November and 5 December. This period was after the SPAW welded to the beach.

to the shoreline the standard deviation of the high tide shoreline showed a similar trend compared to the low tide shoreline, but during the period the SPAW welded to the shoreline there is a sudden decrease of approximately 6 m which was absent for the low tide shoreline. After the decrease the standard deviation increased again to approximately 9 m. The maximum low and high tide locations were also plotted. In Figure 5.6 it can be seen that the maximum low and high tide locations were always located between y = -500 and y = -300 m which corresponded to the seaward protrusion. The maximum shoreline location showed a similar trend as the standard deviation. However, for the high tide shoreline the maximum shoreline location quickly returned to values similar to just before the decrease in the maximum shoreline location during the period of SPAW welding (~20 m).

Based on the low and high tide shorelines the intertidal beach width (IBW) could be determined (Fig. 5.8). The intertidal beach width did not show large variations alongshore besides the inlet located between y = -500 m and y = -700 m until 8 October 2014 (Fig. 5.6). First, the intertidal beach width was around 70 to 80 m between y = -300 m and y = -600 m, but after 8 October 2014, in the period of SPAW welding, the intertidal beach width increased to values around 90 m in this area. The intertidal beach width remained around 90 m until 12 November 2014. In this period the intertidal beach width in the adjacent areas also increased. Hereafter, the intertidal beach width decreased again to values comparable to the period before the SPAW merged with the shoreline (Fig. 5.8A & D). However, the mean location of the intertidal beach was more shoreward now (as shown in Fig. 5.7A & B).

5.3.2 Volume

The alongshore and vertical volume distribution of the intertidal area are shown in Fig. 5.9 and Fig. 5.10, respectively. The alongshore and vertical volume distribution of days 12 August 2014, 26 August 2014, 4 November 2014 and 19 November 2014 were plotted with a dashed line or a transparent bar because these distributions were not realistic (see section 4.5.2). In June and July, the total volume of the intertidal beach was approximately 20.000 m^3 (Fig. 5.10). Before the period the SPAW welded to the beach (before 15 October 2014) the intertidal beach volume slightly increased (~4000 m^3) and the intertidal beach volume was higher between y = -350 m and y = -550 m which coincided with the seaward protrusion of the shoreline (Fig. 5.9). Over time the volume increased in this area from around 40 m^2 to values around 50 m^2 (except 12 and 26 August 2014). The increase of the total intertidal beach volume can also be seen in Figure 5.10. When compared to the period after the SPAW welded to the beach a large part of the volume was present in the lower intertidal area (< 0.50 m). For example, on 29 July 2014 52 % of the total volume was located below 0.50 m compared to only 29 % on 29 October 2014. On 15 October 2014, the first day after the SPAW merged with the beach, the volume increased considerably at y = -500 m to a maximum of 65 m^2. After that the peak around y = -500 m disappeared and a considerable increase occurred between y = -400 and y = -200 m with maximum values around 60 m^2. The vertical volume distribution in this period shows that the total volume increased to almost 26,500 m^3 on 15 October 2014 and to almost 30,000 m^3 on 23 October 2014 which corresponded with an onshore sediment flux of ~2.0 m^3/m/day between y = -550 m and y =-350 m. In the following period the total volume was similar on 29 October 2014 and 9 November 2014. When looked at the vertical distribution of the intertidal beach volume it seemed that after the SPAW welded to the beach the volume especially was present in the more landward part of the intertidal area (> 0.50 m). In the following period the sand volume in the more landward part of the intertidal beach seemed to increase even more while the sand volume in the lower part of the intertidal area seemed to decrease.

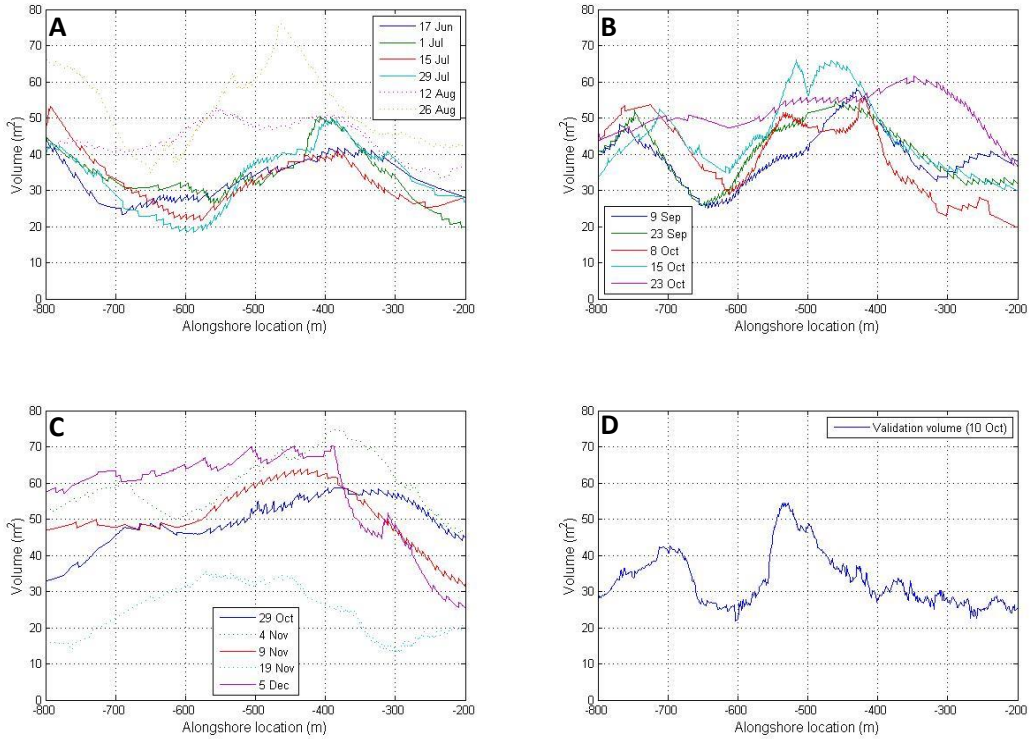

Figure 5.9. The alongshore volume distribution (m²) of the intertidal area (-0.25 m – 1.41 m) over time (in 2014) of the interpolated shorelines and validation data. A) Alongshore volume distribution of 17 June, 1 July, 15 July, 29 July, 12 August and 26 August. This period included the period of SPAW emergence. B) Alongshore volume distribution of 9 September, 23 September, 8 October, 15 October and 23 October. This period included the period of SPAW welding. C) Alongshore volume distribution of 29 October, 4 November, 9 November, 19 November and 5 December. This was the period after SPAW welding. D) The alongshore volume distribution of the validation data collected with the MLS collected on 10 October 2014. The dashed lines represent data which were considered unreliable (see section 4.5.2).

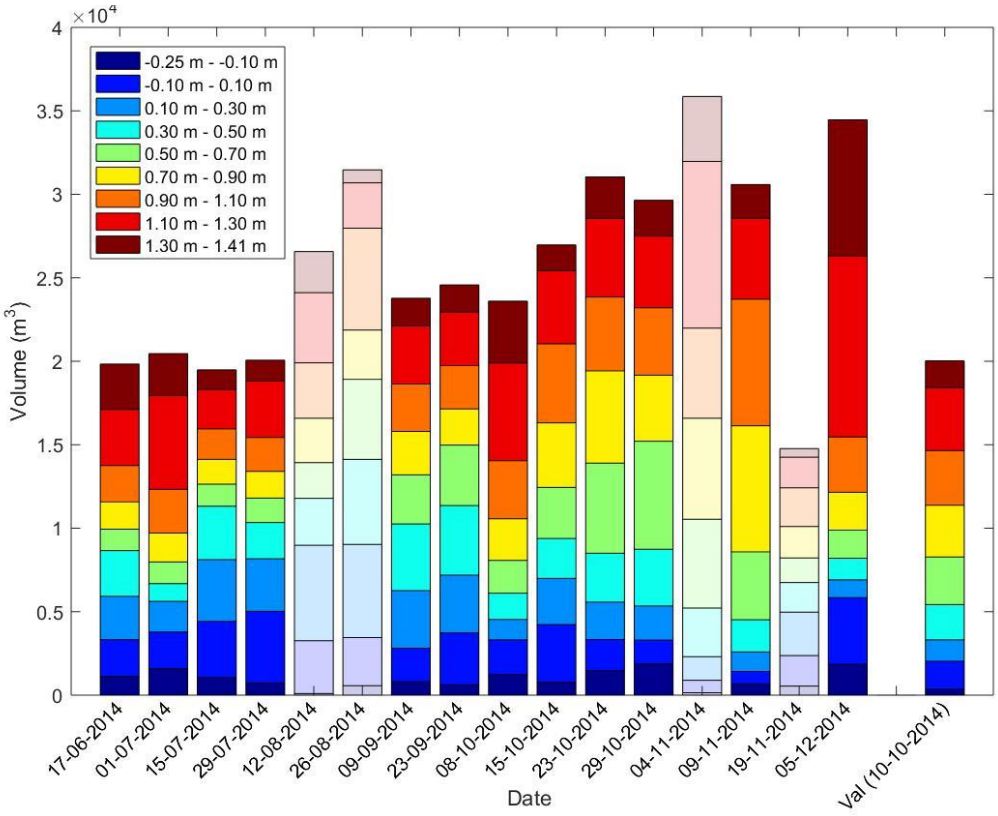

Figure 5.10. The vertical volume distribution of the intertidal area (-0.25 m – 1.41 m) for all mapped days. The last bar represents the validation data (see section 4.6). Each box represents the volume between two elevations. All the boxes combined represent the total intertidal beach volume for that day. The more transparent bars represent data which were considered unreliable (see section 4.5.2).

Chapter 6 Discussion

6.1 Model evaluation & comparison

To compare the classified shorelines and interpolated bathymetries to data from other studies, the main assumptions and uncertainties stated in Chapter 4 are briefly summarized first. Unfortunately, no GPS-surveyed shorelines were available to validate the classified shorelines. However, to give an indication of the reliability of the IBM, the validation of shoreline points classified with the IBM by Aarninkhof et al. (2003) will be discussed. The mean absolute vertical offset was less than 15 cm along more than 85% of the 2-km-long stretch of beach they mapped. This vertical offset corresponds to a mean horizontal offset of 6 m. The mean vertical offset for the whole area was -8.5 cm with a standard deviation of 17.4 cm. This means the shoreline points showed a landward offset. This was largely compensated by a mean elevation induced offset of 7.8 cm which had a standard deviation of 12.6 cm (Aarninkhof et al., 2003). In general, the further away the shoreline points were from the Argus camera the larger the model deviations. This was caused by a decrease of pixel resolution further away from the camera. Because of the more careful classification of shorelines in this study the shoreline points are expected to be more accurate than found by Aarninkhof et al. (2003).

The tidal range was not equal on each day. The tidal range varies per cycle, but also the tidal range captured in the images was dependent on the moments the images were taken. Therefore, the tidal range was set between -0.18 m and 0.99 m. All low and high water levels did not vary more than 0.05 m from these values. Still, these deviations could affect the intertidal beach width in the order of one to several tens of meters.

The shoreline points were interpolated with a loess interpolation using L_x = 20 m and L_y = 150 m (Plant et al., 2002). Factors like the number of classified shorelines per day, manually added shoreline points, a non-equally-spaced grid, loss of pixel resolution further from the camera, the deviation of high tide elevations, low tide elevations and/or tidal range could have affected the interpolation (see section 4.5.2).

The interpolated bathymetry of 8 October 2014 was validated against ground truth data obtained with an MLS on 10 October 2014. It was assumed the change in morphodynamics in these two days was minor. The mean difference between the two bathymetries was -2.2 cm with a standard deviation of 0.17 m. The RMSE was also 0.17 m. The landward edges of the area showed a large underestimation of the elevation (Fig. 4.5D) and corresponded to high interpolation errors (Fig. 4.5C). Overestimation was especially located adjacent to the seaward protrusion. The validation volume was 19,552 m^3 and the interpolated volume of the same area was 16,301 m^3. This indicates an underestimation of the volume.

Plant et al. (2007) also classified the shoreline at Egmond with the PIC model and found an RMSE error of the shoreline points of 0.17 m. An RMSE of 0.17 m was also found in this study, but this was the RMSE of the whole interpolated bathymetry and not only the shoreline points. This means the shoreline points classified in this study are probably more reliable than the shoreline points mapped by Plant et al. (2007). Also, it should be noted that the data return percentage at Egmond was only 24 % for the 44 images classified by Plant et al. (2007). This means only a small portion of the used images could be classified. In this study 96 % of the available images on the day used for validation

was classified. The higher reliability and data return percentage could be related to the more careful classification of the shorelines.

Uunk (2008) tried to further develop the Automated Shoreline Mapper (ASM) which is an automated version of the IBM. From the shoreline points, bathymetries were determined by a loess interpolation. To compare the interpolated bathymetry determined by the IBM and by the ASM the bathymetries were compared to DGPS data. Uunk (2008) used three different smoothing scales: L_x = 10 m and L_y = 25 m, L_x = 10 m and L_y = 100 m, and L_x = 25 m and L_y = 100 m. For one day the RMSEs were 0.25 m, 0.27 m and 0.32 m, respectively. These errors are large compared to the RMSE found in this study. The lower RMSE could again be related to the more careful classification of the shorelines in this study.

6.2 Effects of a SPAW event on the intertidal beach and shoreline

6.2.1 Period before SPAW event

The shoreline in the study area already showed alongshore variability before the SPAW emerged. It is not known why there was already a clear embayment in the shoreline of the Egmond area between y = -1200 and y = 500 m (Fig. 5.1). Begin 2014 the inner bar seemed straight alongshore with no or little coupling to the shoreline. However, the inner bar developed a highly 3D crescentic pattern in the following period and the development of mega-cusp embayments was initiated. Moreover, an out-of-phase coupling between the inner bar and the shoreline developed (Fig. 5.4). So, the horns of the inner bar corresponded with the horns of the shoreline. In the centre of the embayment also a protrusion of the shoreline developed (Fig. 5.2 & 5.4). In the period before the SPAW emerged the mean shoreline position decreased because the intertidal bar migrated onshore. The standard deviation was stable until around June 2014 (Fig. 5.5B). Then the alongshore variability of the inner bar possibly induced a circulation current landward of the inner bar which was also modelled by Castelle et al. (2010). This circulation resulted in morphological change of the shoreline. The formation of the seaward protrusion in the study area caused the standard deviation to increase. For the data obtained with the IBM, only 17 June 2014 was dated in the period before the SPAW event. So, no trends could be discussed, but it can be said that the formation of the seaward protrusion resulted in a higher intertidal beach width and larger volume at that location in the study area (Fig. 5.8 & 5.9).

6.2.2 Period after SPAW emergence

After the SPAW emerged from the inner bar the standard deviation of the high and low tide line did show an increase (Fig. 5.5B, 5.7C & 5.7D). So, the alongshore variability in the study area increased. The reason the values collected with the IBM and BLIM were not the same is that with the BLIM the white foam patch near the low tide line was mapped while with the IBM the actual shoreline was mapped. In Figure 5.6 it can be seen that the white foam patch was located more seaward and showed little alongshore variability while the actual shoreline was located more shoreward and was more variable alongshore. Even though the inner bar straightened after the SPAW emerged, the circulation pattern probably remained present because still more waves broke over the SPAW. This circulation was also found in the modelling study of Van der Weerd (2012) (Fig. 6.1). The circulation pattern was stronger when the SPAW was located further away from the shoreline (Van der Weerd, 2012). The SPAW migrated barely during this period, only just before the SPAW welded to the beach the migration speed increased. A similar migration pattern was documented by De Wit (2017). The

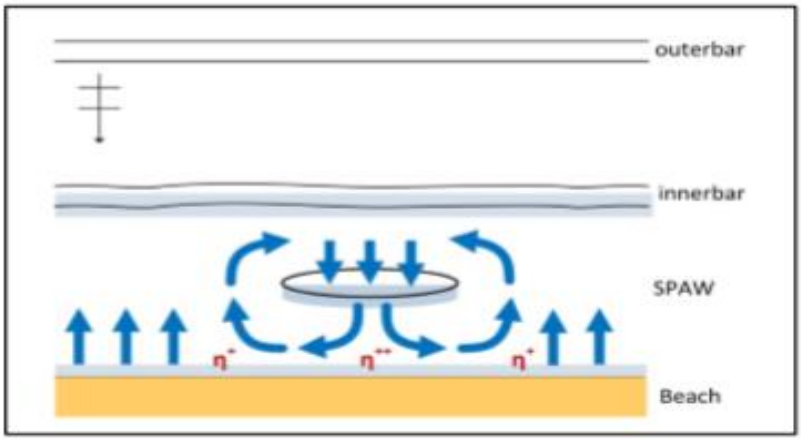

Figure 6.1. Schematized horizontal circulation cell induced by local pressure gradients due to wave breaking. η+ indicate areas of set up, η+ indicate areas of large set-up. Blue arced areas indicate wave breaking. (Van der Weerd, 2012).

high migration speed coincided with larger wave heights (2-3 m on 7 – 9 October 2014) (Fig. 5.3C). In the period after SPAW emergence, the SPAW had many similarities with shoreface nourishment behaviour, except nourishments are generally larger. Just like with a nourishment a lee and feeder effect occurred. Therefore, the shoreline protruded more seaward behind the SPAW while the adjacent areas retreated more landward (Van Rijn & Walstra, 2004). The narrowing of the seaward protrusion of the shoreline was probably related to the dimensions of the SPAW compared to the dimensions of the inner bar horn. The alongshore dimension of the horn of the inner bar was probably larger than the alongshore dimension of the SPAW. Therefore, a larger part of the shoreline was affected by the horn. The increase in alongshore variability already began before the SPAW emerged from the inner bar and was thus not only an effect of the SPAW. However, the effect of the inner bar and the SPAW on the intertidal beach and shoreline was different. After the emergence of the SPAW the standard deviation of the shoreline showed a larger increase than before SPAW emergence (5.5B). Also, the emergence of the SPAW resulted in a larger sand input to the beach and consequently an increase of the intertidal beach volume (Fig. 5.10). The mean position of the shoreline did decrease until the moment the SPAW merged with the shoreline because the intertidal bar kept migrating onshore. However, a small deviation from this decrease could be seen around the moment of SPAW emergence. This short stagnation of the onshore migration of the low tide line was possibly related to a change in hydrodynamics when the SPAW formed.

The high tide line showed another response than the low tide line. The mean high tide level remained stable, but the standard deviation of the high tide level did increase (Fig. 5.7). The stable mean high tide line location means the sediment which was deposited in the upper intertidal area at the location of the SPAW was counteracted by the retreat of the mean high tide line in adjacent areas. The reason can be seen in Figure 5.6. An inlet is present next to the SPAW location. The inlet drains the trough landward of the intertidal bar. During high tide this inlet acted as a rip current. The circulation during high tide resulted in the deposition of sediment landward of the protrusion and erosion landward of the inlet (Fig. 5.9A & B). On the other side of the seaward protrusion the high tide line showed minor change. The volume of the intertidal beach remained equal in the first period (~20,000 m^3) (Fig 5.10). However, the volume of the intertidal beach suddenly considerably increased on 12 and 26 August 2014. The volumes computed for those days were regarded as

incorrect (see section 4.5.2). The errors on these days were related to the tidal range that was covered in the Argus images. When these volumes were ignored, an increase in volume of ~4000 m^3 could be seen which can again be related to the lee effect of the SPAW. In this period most of the sand volume was located in the lower part of the intertidal area. The alongshore extent of the area affected by the SPAW was approximately 500 meters (Fig. 5.9).

6.2.3 Period after the SPAW welded to the beach

The impact of the welding of the SPAW to the beach can be clearly seen (Fig. 5.5, 5.7, 5.8, 5.9 & 5.10). The mean low tide line immediately moved seaward, the standard deviation of the low tide line decreased, the intertidal beach width increased at the location where the SPAW merged with the beach and the total volume of the intertidal area increased (Fig. 5.5, 5.8 & 5.10). It was assumed the SPAW merged with the shoreline between 8 October 2014 and 15 October 2014. The length and width of the SPAW, 175 m and 20 m respectively, were similar to the mean length and width found by Wijnberg and Holman (2007) and Price et al. (2017), namely 126 m and 30 m, and 200 m and 30 m, respectively. These dimensions were also based on the visible foam patch in the Argus imagery. Price et al. (2017) also determined the dimensions of one SPAW event with the help of bathymetric maps. The average length and width found were much larger, namely 300 m and 70 m respectively. The dimensions of the SPAW analysed in this study were probably larger because the lower parts of the SPAW did not cause wave breaking and therefore no foam was visible at the surface. The volume increase on the intertidal beach after the SPAW welded to the beach reached up to 6,000 m^3 over the alongshore extent of the study site. This was not the total volume of the SPAW because the volume was only calculated above -0.25 m. In the area which was located below -0.25 m also sand of the SPAW was deposited. The volumes based on the foam patch in the timex images were 6,000 m^3 at Egmond and 1,900 m^3 at Duck (Wijnberg and Holman, 2007; Price et al., 2017). These could therefore be considered as an underestimation. The real volume of the SPAW near the coast was expected to be more in the range of the volume found by the assimilation model, so between 10,000 and 20,000 m^3 (De Wit, 2017). The onshore sediment flux during the period of SPAW welding found in this study (~2.0 m^3/m/day) was similar to the onshore sediment flux found by Wijnberg and Holman (2007) and Van der Weerd (2012) which were 1 to 2 m^3/m/day and 1.3 m^3/m/day, respectively.

The SPAW caused a large input of sediment to the beach which extended the shoreline more seaward (Fig. 5.8 & 5.9). The high decrease in the standard deviation could be explained by looking at the morphological evolution of the beach. Figure 5.6 shows that the SPAW merged with the shoreline between y = -600 m and y = -350 m. However, after this the sediment quickly dispersed along the coast which resulted in a more uniform intertidal beach width alongshore (Fig. 5.8). In less than a month the seaward protrusion was already dispersed over the whole extent of the study area. As a result, a new intertidal bar developed and the standard deviation of the low tide line decreased (Fig. 5.5B & 5.7C). As possible explanation for the formation of an intertidal bar could be that there was a depression between the centre of the SPAW and the intertidal beach. Somehow, in this depression a current was able to maintain itself during high water while the sand of the SPAW was dispersed alongshore. Whether the formation of an intertidal bar is typical after a SPAW welds to the beach is not sure because the formation of the intertidal bar could also be related to the storm which occurred just after the SPAW welded to the beach. The high tide line showed a totally different trend after the SPAW welded to the beach. A sudden decrease in the mean high tide line and standard deviation of the high tide line can be seen in Figure 5.7. An explanation for this quick

drop were the very high wave conditions (H_s > 6 m) occurring on 21 October 2014 (Fig. 5.3C). The upper part of the intertidal beach was partly eroded, especially at the alongshore location where the SPAW merged. It should be expected that a decrease in intertidal beach volume was present. However, this is not seen in Figure 5.10. The sand volume on the upper part of the intertidal beach and also for the whole intertidal beach even seemed to increase. A possible explanation can be found in Figure 5.9. Here it can be seen that the volume did indeed decrease at the alongshore location where the SPAW merged, but between y = -400 m and y = -200 m a large increase in volume can be seen. The offshore angle of wave incidence relative to shore-normal varied between 30° and 60° during this storm (Fig. 5.3F). Therefore, a strong alongshore current was generated which transported the sediment south resulting in erosion landward of the location the SPAW merged with the shoreline and deposition south of this area. After the storm the mean and the standard deviation of the high tide line increased again (5.7B & D). Thus, the sudden decrease in the mean and the standard deviation of the high tide line were not related to the merging of the SPAW. The seaward protrusion of the low water line was still present after the storm, but migrated south (Fig. 5.6). At the location of the seaward protrusion the high tide line also developed a more seaward protrusion. A seaward migration of the high tide line means that the sand volume on the dry beach increased which could be related to an increase of intertidal beach width which was also found by Aagaard et al. (2004) and Anthony et al. (2006). This could also be seen in the vertical sediment volume distribution of the intertidal beach (Fig. 5.10). This means there was a sediment flux from the (lower) intertidal beach to the upper dry beach. The development of the beach after the storm was different from the situation studied by Aagaard et al. (2004) where an intertidal bar merged with the shoreline. In Figure 2.8 it could be seen that under similar wind conditions the sediment transport was much larger when the intertidal bar merged with the beach. Therefore, it is expected the impact on the dunes was considerable. Here, also the intertidal beach width increased after the merging which resulted in an increase of aeolian transport. The sand from the lower intertidal beach was transported to the upper intertidal beach which probably also happened after the SPAW merged. However, after a storm the intertidal bar was completely eroded and the intertidal beach width decreased again. This was not the case for the Egmond coast. There was a lot of erosion, but still the impact of the SPAW after it welded with the beach on the dimensions of the intertidal beach was still present. This probably indicates that the sediment input caused by the merging of the SPAW must have been large enough to not get totally eroded during one storm.

Unfortunately, there is a data gap after 12 December 2014 until 7 April 2015. Therefore, it is hard to say what happened on the long term and how long the effect of the SPAW lasted. In the period after the data gap the embayment was still present and became wider (Fig. 5.2). The seaward protrusion also became wider and deviated less from the smoother shoreline. This probably means that the dispersion of the SPAW sediment continued in this period. The mean shoreline location was still higher on 7 April 2015 which means the mean shoreline location kept migrating more seaward (Fig. 5.5A). How long this process lasted is unknown. This is also the case for the standard deviation of the shoreline location. When the data were available again the standard deviation of the shoreline location was still lower than before the data gap (Fig. 5.5B). However, again it was unknown how long this effect lasted. Still, it could be said that the effect of the SPAW on the intertidal beach ended before 7 April 2015 because the trends hereafter were different than the period just after the SPAW welded to the beach. So, the effect of the SPAW event on the intertidal beach lasted between 2 and 6 months.

The effect of this SPAW could be seen in the mean shoreline location and the standard deviation of the shoreline location for the whole area (Fig. 5.5). However, multiple SPAW events occurred in 2014, but the effect of other SPAWs could not be easily detected. The impact of a SPAW or detectability of this impact was therefore probably dependent on its dimensions, but also on the morphological setting of the initial intertidal beach.

Conclusions and Recommendations

7.1 Conclusions

The impact of a SPAW on the intertidal beach characteristics was studied using Argus imagery of Egmond beach. From these Argus images shorelines were mapped each one or two weeks between 17 June 2014 and 5 December 2014 with the Intertidal Beach Mapper (IBM). Moreover, daily shorelines obtained with the BarLine Intensity Mapper (BLIM) were available. Two periods were studied in which the SPAW affected the intertidal beach: the period after the SPAW emerged from the inner bar and did not yet merge with the beach and the period after the SPAW merged with the beach. Furthermore, the distribution of the sediment of the SPAW in cross-shore and alongshore direction was studied for these periods.

Before the SPAW emerged from the inner bar, the shoreline already showed alongshore variability in the form of an approximately 1800 m wide embayment which was located approximately 10 to 20 m more shoreward than the rest of the shoreline. In the centre of this embayment there was a small seaward protrusion of the shoreline which extended approximately 5 m more seaward than the embayment and was coupled with a horn of the inner bar. At this location a SPAW would eventually split from the inner bar in begin July 2014. The SPAW migrated onshore and caused the seaward protrusion to extend even further seaward (~20 m) while the adjacent areas would show a retreat of the shoreline (~15 m). This was caused by circulation current induced by the SPAW. The alongshore variability of the location of the low tide line and the high tide line both increased in the period after SPAW emergence but before SPAW welding, from approximately 5 m to 30 m and 6 m to 12 m respectively. However, while the low tide line migrated approximately 20 m onshore because of the landward migration of the intertidal bar, the high tide line location remained stable around -5 m. Despite, the decrease in low tide line location the intertidal beach width did increase with 10 to 20 m at the location of the seaward protrusion. In addition, the intertidal beach volume increased with approximately 4000 m^3, especially between y = -550 m and y = -350 m, and most of the sand was located in the lower intertidal area (52% < 0.50 m on 29 July 2014).

The welding of the SPAW to the beach resulted in a large sediment input to the intertidal beach. The volume of the intertidal beach (-0.25 m to 1.41 m) increased with ~6,000 m^3, and the intertidal beach width increased with 5 to 15 m on an alongshore distance of 300 m. During the period of SPAW welding the alongshore volume increased from 40-50 m^2 to a maximum of 65 m^2 in this area. The onshore sediment flux was ~2.0 m^3/m/day. The mean high tide line and the mean low tide line both migrated seaward. The alongshore variability of the low tide line decreased from 30 m to 15 m in only two months because the accumulated sand of the merged SPAW quickly was dispersed in alongshore direction. A new intertidal bar was formed and in less than a month the sand was dispersed over the whole study area (~600 m). Sand was not only transported alongshore. Because the intertidal beach width increased after the SPAW welded to the beach the aeolian transport potential on the beach increased. Sand from the lower part of the intertidal beach was transported to the upper part of the intertidal beach (61 % > 0.50 m on 25 October 2014) and even further shoreward. Therefore, the alongshore variability in the high tide line position increased from approximately -10 m to 5 m.

The long term effect of the SPAW on the intertidal beach is uncertain because these data were absent. However, it can be said that the effect of the SPAW on the mean shoreline position and its

alongshore variability lasted between 2 and 6 months because after the data gap the trends were similar to the period before the SPAW emerged and the seaward protrusion could not be distinguished anymore.

7.2 Recommendations

To better understand the impact of SPAWs on the beach more SPAW events should be studied. In this study only one SPAW event was studied because the classification of the shorelines was very time consuming. The impact of this SPAW was clearly visible in the changing dimensions of the intertidal beach. However, other SPAW events occurred in 2014 which did not seem to really impact the intertidal beach dimensions. Further research can shed light on this different response of the intertidal beach.

Furthermore, the effect of the local input of sediment and the increase in beach width induced by the merged SPAW on aeolian transport and dune development should be studied. This study showed there was a considerable amount of sediment transported in cross-shore and longshore direction which could locally strengthen the dune system. In addition, the study of Aagaard et al. (2004) showed that the welding of an intertidal bar had a large effect on the aeolian transport which could also be the case for the welding of a SPAW. When comparing this to areas without a merging SPAW the impact on the dunes can be established.

The volumes calculated in this study showed a lot of uncertainty. Some bathymetries which were interpolated from the mapped shorelines did show large deviations from the surrounding days. These deviations were often related to the low tide and high tide covered in the images on a day. For more reliable results, classification days with similar wave heights should be chosen. Also, these days should have a similar tidal range.

To better understand the whole effect of SPAWs on the intertidal beach, other SPAW events with more data should be studied. One possibility is to intensively monitor one SPAW event. When a SPAW event is detected the beach elevation could be monitored during low tide with a drone or MLS. These surveys should begin after SPAW emergence and should be repeated for example every two weeks until three months after SPAW welding. However, this is probably very time consuming and expensive, but it does give a clear overview of the development of the intertidal beach and therefore the impact of the SPAW. Another option is trying to model SPAWs. Castelle (2004) did obtain a feature similar to a SPAW in his modelling study. This could be combined with models used to study nourishment behaviour. The combination of these models would then include the formation, migration and welding of the SPAW.

References

Aagaard, T., Davidson-Arnott, R., Greenwood, B., & Nielsen, J. (2004). Sediment supply from shoreface to dunes: linking sediment transport measurements and long-term morphological evolution. Geomorphology, 60(1), 205-224.

Aagaard, T., Kroon, A., Andersen, S., Sørensen, R. M., Quartel, S., & Vinther, N. (2005). Intertidal beach change during storm conditions; Egmond, The Netherlands. Marine geology, 218(1): 65-80.

Aagaard, T., Nielsen, J., Davidson-Arnott, R., Greenwood, B. & Nielsen, N. (1998a). Coastal morphodynamics at Skallingen, SW Denmark: high energy conditions. Danish Journal of Geography 98, 20–30.

Aagaard, T., Nielsen, J., & Greenwood, B. (1998b). Suspended sediment transport and nearshore bar formation on a shallow intermediate- state beach. Marine Geology 148, 203– 225.

Aarninkhof, S. G. J. (2003). Nearshore bathymetry derived from video imagery, Delft University of Technology, The Netherlands, PhD thesis, 175p.

Aarninkhof, S. G. J. (2004). Praktische Facetten Inzet Argus. Deltares WL, Z3781.

Aarninkhof, S. G. J., & Roelvink, J. A. (1999). Argus-based monitoring of intertidal beach morphodynamics. Proc. of Coastal Sediments Conf., Long Island (NY), USA, pp. 2429 – 2444.

Aarninkhof, S. G. J., Ruessink, B. G., & Roelvink, J. A. (2005). Nearshore subtidal bathymetry from time-exposure video images. *Journal of Geophysical Research: Oceans*, *110*(C6).

Aarninkhof, S. G. J., Turner, I. L., Dronkers, T. D. T., Caljouw, M., & Nipius, L. (2003). A video-based technique for mapping intertidal beach bathymetry. *Coastal Engineering,* 49(4), 275–289.

Almar, R., Castelle, B., Ruessink, B. G., Sénéchal, N., Bonneton, P. & Marieu, V. (2010). Two-and three-dimensional double-sandbar system behaviour under intense wave forcing and a meso–macro tidal range. Continental Shelf Research, 30(7) : 781-792.

Almar, R., Coco, G., Bryan, K. R., Huntley, D. A., Short, A. D., & Senechal, N. (2008). Video observations of beach cusp morphodynamics. Marine geology, 254(3), 216-223.

Anthony, E. J., Ruz, M. H., & Vanhée, S. (2009). Aeolian sand transport over complex intertidal bar-trough beach topography. *Geomorphology*, *105*(1-2), 95-105.

Anthony, E. J., Vanhee, S., & Ruz, M. H. (2006). Short-term beach–dune sand budgets on the north sea coast of France: Sand supply from shoreface to dunes, and the role of wind and fetch. Geomorphology, 81(3), 316-329.

Battjes, J. A., & Janssen, J. P. F. M. (1978). Energy loss and set-up due to breaking in random waves. Proc. of 16th Int. Conf. on Coastal Eng. ASCE, New York, pp. 569– 587.

Boczar-Karakiewicz, B., & Davidson-Arnott, R. G. D. (1987). Nearshore bar formation by non-linear wave processes— A comparison of model results and field data. Marine Geology 77, 287–304.

Bowen, A. J. (1980). Simple models of nearshore sedimentation, beach profiles and longshore bars. In: McCann, S.B. (Ed.), The Coastline of Canada, Geological Survey of Canada Paper, vol. 80-10, pp. 1 –11.

Bowman, D., & Goldsmith, V. (1983). Bar morphology of dissipative beaches: an empirical model. *Marine Geology*, *51*(1-2), 15-33.

Brander, R. W. (1999). Field observations on the morphodynamic evolution of a low-energy rip current system. *Marine geology*, *157*(3-4), 199-217.

Castelle, B. (2004). Modélisation de l'hydrodynamique sédimentaire au-dessus des barres sableuses soumises à l'action de la houle: application à la côte aquitaine. Ph.D. Thesis, Université Bordeaux I, 340p.

Castelle, B., Bonneton, P., Dupuis, H., & Sénéchal, N. (2007). Double bar beach dynamics on the high-energy meso-macrotidal French Aquitanian Coast: a review. *Marine geology*, *245*(1-4), 141-159.

Castelle, B., Marieu, V., Bujan, S., Splinter, K. D., Robinet, A., Sénéchal, N., & Ferreira, S. (2015). Impact of the winter 2013–2014 series of severe Western Europe storms on a double-barred sandy coast: Beach and dune erosion and megacusp embayments. Geomorphology, 238, 135-148.

Castelle, B., Ruessink, B. G., Bonneton, P., Marieu, V., Bruneau, N., & Price, T. D. (2010). Coupling mechanisms in double sandbar systems. Part 1: Patterns and physical explanation. *Earth Surface Processes and Landforms*, *35*(4), 476-486.

Christiansen, M. B. & Davidson-Arnott, R. (2004). Rates of landward sand transport over the foredune at Skallingen, Denmark and the role of dune ramp. Danish Journal of Geography 104, 31–43.

Coco, G. (2017). Beach Cusps. In Atlas of Bedforms in the Western Mediterranean (pp. 55-57). Springer International Publishing.

Coco, G., Bryan, K. R., Green, M. O., Ruessink, B. G., van Enckevort, I. M., & Turner, I. L. (2005). Video observations of shoreline and sandbar coupled dynamics. In Coasts and Ports 2005: Coastal Living-Living Coast; Australasian Conference; Proceedings (p. 471). Institution of Engineers, Australia.

Dally, W. R., & Dean, R. G. (1984). Suspended sediment transport and beach profile evolution. Journal Waterway, Port, Coastal and Ocean Engineering 110, 15– 33.

Davidson-Arnott, R. G. D. (1981). Computer simulation of nearshore bar formation. Earth Surface Processes and Landforms 6, 23– 34.

Davidson-Arnott, R. G. D., & McDonald, R. A. (1989). Nearshore water motion and mean flows in a multiple parallel bar system. Marine Geology 86, 321–338.

Davidson-Arnott, R. G. D., & Pember, G. F. (1980). Morphology and sedimentology of multiple parallel bar systems, Southern Georgian Bay, Ontario. In: McCann, S.B. (Ed.), The Coastline of Canada, Geological Survey of Canada Paper, vol. 80-10, pp. 417– 428.

Davis, R.A., Fox, W. T., Hayes, M. O., & Boothroyd, J. C. (1972). Comparison of ridge and runnel systems in tidal and non-tidal environments. Journal of Sedimentary Petrology 2, 413– 421.

Dawson, J. C., Davidson-Arnott, R. G. D., & Ollerhead, J. (2002). Low energy morphodynamics of a ridge and runnel system. Journal of Coastal Research SI 36, 198– 215.

De Winter, R. C., Gongriep, F., & Ruessink, B. G. (2015). Observations and modeling of alongshore variability in dune erosion at Egmond aan Zee, the Netherlands. Coastal Engineering, 99: 167-175. doi: http://dx.doi.org/10.1016/j.coastaleng.2015.02.005

De Wit, L. (2017). Objective detection and quantitative analyses of a Shoreward Propagating Accretionary Wave in a double sandbar system (MSc Thesis). Utrecht University, 72p.

Dolan, R., Hayden, B. P., May, P., & May, S. K. (1980). The reliability of shoreline change measurements from aerial photographs. Shore and Beach, 48(4), 22–29.

Dolan, T. J., & Dean, R. G. (1985). Multiple longshore sand bars in the upper Chesapeake Bay. *Estuarine, Coastal and Shelf Science*, *21*(5), 727-743.

Donker, J. J. A., Hage, P. M. & Ruessink, B.G. (2016). Dune recovery and development in the aftermath of the Sinterklaasstorm. Not published.

Exon, N. F. (1975). An extensive offshore sand bar field in the western Baltic Sea. Marine Geology 18, 197– 212.

Falqués, A., & Ribas, F. (2017). Km-Scale Shoreline Sand Waves. In Atlas of Bedforms in the Western Mediterranean (pp. 59-63). Springer International Publishing.

Greenwood, B., & Davidson-Arnott, R. G. D. (1975). Marine bars and nearshore sedimentary processes, Kouchibouguac Bay, New Brunswick, Canada. Nearshore sediment dynamics and sedimentation, 16, 123-150.

Greenwood, B., & Davidson-Arnott, R. G. D. (1979). Sedimentation and equilibrium in wave-formed bars: a review and case study. Canadian Journal of Earth Sciences 16, 312–332.

Guillén, J., Stive, M.J.F. & Capobianco, M. (1999). Shoreline evolution of the Holland coast on a decadal scale. Earth Surface Processes and Landforms 24, 517–36.

Haas, K. A., Svendsen, I. A., Haller, & M. C., Zhao, Q. (2003). Quasi-threedimensional modelling of rip currents systems. Journal of Geophysical Research 108(C7): 3217. DOI: 10.1029/2002JC001355

Holland, K. T., Holman, R. A., Lippmann, T. C., Stanley, J., & Plant, N. G. (1997). Practical use of video imagery in nearshore oceanographic field studies. IEEE Journal of Oceanic Engineering 22 (1), 81–92.

Holman, R. A., & Sallenger, A. H. (1985). Setup and swash on a natural beach. Journal of Geophysical Research 90, 945– 953.

Holman, R. A., & Stanley, J. (2007). The history and technical capabilities of Argus. *Coastal Engineering*, *54*, 477-491.

Keijsers, J. G., Poortinga, A., Riksen, M. J., & Maroulis, J. (2014). Spatio-temporal variability in accretion and erosion of coastal foredunes in the netherlands: Regional climate and local topography. PloS one, 9(3), e91115.

King, C. A. M. (1972). Beaches and Coasts, 2nd edition. Edward Arnold, London.

King, C. A. M., & Williams, W. W. (1949). The formation and movement of sand bars by wave action. *The Geographical Journal*, *113*, 70-85.

Kingston, K. S. (2003). Applications of complex adaptive systems, approaches to coastal systems. Plymouth, UK: University of Plymouth, PhD thesis, 106 p.

Komar, P. D. (1971). Nearshore cell circulation and the formation of giant cusps. Geological Society of America Bulletin 82: 2643–2650.

Konicki, K. M. & Holman, R. A. (2000). The statistics and kinematics of transverse bars on an open coast. Marine Geology, 169: 69–101.

Kroon, A. (1994). Sediment Transport and Morphodynamics of the Beach and Nearshore Zone near Egmond, The Netherlands. PhD thesis, Utrecht University.

Kroon, A., & Masselink, G. (2002). Morphodynamics of intertidal bar morphology on a macrotidal beach under low-energy wave conditions, North Lincolnshire, England. Marine Geology 190, 591– 608.

Levoy, F., Anthony, E. F., Barusseau, J. P., Howa, H., & Tessier, B. (1998). Morphodynamics of a macrotidal ridge and runnel beach. C. R. Academie des Sciences 327, 811– 818.

Lippmann, T. C. & Holman, R. A. (1989). Quantification of sand bar morphology: a video technique based on wave dissipation. Journal of Geophysical Research, 94:995–1011.

Masselink, G. (1993). Simulating the effects of tides on beach mophodynamics. Journal of Coastal Research, 15, 180-197.

Masselink, G., & Anthony, E.J. (2001). Location and height of intertidal bars on macrotidal ridge and runnel beaches. Earth Surface Processes and Landforms 26, 759– 774.

Masselink, G., Kroon, A., & Davidson-Arnott, R. G. D. (2006). Morphodynamics of intertidal bars in wave-dominated coastal settings - A review. Geomorphology, 73(1), 33-49.

Masselink, G., & Pattiaratchi, C. B. (1998). Morphological evolution of beach cusps and associated swash circulation patterns. Marine Geology, 146(1), 93-113.

Masselink, G., & Short, A. D. (1993). The effect of tide range on beach morphodynamics and morphology: a conceptual beach model. Journal of Coastal Research, 9(3): 785-800.

Masselink, G., & Turner, I. L. (1999). The effect of tides on beach morphodynamics. In: Short, A.D. (Ed.), Handbook of Beach and Shoreface Morphodynamics. Wiley, Chichester, pp. 204– 229.

Mulrennan, M. E. (1992). Ridge and runnel beach morphodynamics: an example from the Central East Coast of Ireland. Journal of Coastal Research 8, 906– 918.

Orford, J. D., & Wright, P. (1978). What's in a name? Descriptive or genetic implications of 'ridge and runnel' topography. Marine Geology 28, M1–M8.

Orzech, M. D., Reniers, A. J., Thornton, E. B., & MacMahan, J. H. (2011). Megacusps on rip channel bathymetry: Observations and modeling. Coastal Engineering, 58(9), 890-907.

Owens, E. H., & Frobel, D. H. (1977). Ridge and runnel systems in the Magdalen Islands, Quebec. Journal of Sedimentary Petrology 47, 191–198.

Pape, L. (2008). BLIM Toolbox manual. *IMAU Report R08-02.*

Plant, N. G., Aarninkhof, S. G. J., Turner, I. L., & Kingston, K. S. (2007). The performance of shoreline detection models applied to video imagery. *Journal of Coastal Research*, 658-670.

Plant, N. G., Holland, K. T., & Puleo, J. A. (2002). Analysis of the scale of errors in nearshore bathymetric data. *Marine Geology*, *191*(1-2), 71-86.

Plant, N. G., & Holman, R. A. (1997). Intertidal beach profile estimation using video images. *Marine Geology,* 140, 1–24.

Price, T. D., & Ruessink, B. G. (2008). Morphodynamic zone variability on a microtidal barred beach. Marine Geology, 251(1), 98-109.

Price, T. D., & Ruessink, B. G. (2011). State dynamics of a double sandbar system. *Continental Shelf Research*, *31*(6), 659-674.

Price, T. D., & Ruessink, B. G. (2013). Observations and conceptual modelling of morphological coupling in a double sandbar system. Earth Surface Processes and Landforms, 38(5), 477-489.

Price, T. D., van Kuik, N., de Wit, L., Dionísio António, S., & Ruessink, B. G. (2017). Shoreward Propagating Accretionary Waves (SPAWs): Observations from a multiple sandbar system. In Proceedings Coastal Dynamics 2017 (pp. 1081-1089).

Quartel, S. (2009). Temporal and spatial behaviour of rip channels in a multiple-barred coastal system. Earth Surface Processes and Landforms 34: 163–176.

Roelvink, J. A., & Stive, M. J. F. (1989). Bar-generating cross-shore flow mechanisms on a beach. Journal of Geophysical Research 94, 4785–4800.

Ruessink, B. G., & Jeuken, M. C. J. L. (2002). Dunefoot dynamics along the Dutch coast. Earth Surface Processes and Landforms, 27(10), 1043-1056.

Ruessink, B. G., Kleinhans, M. G., & Van Beukel, P. G. L. (1998). Observations of swash under highly dissipative conditions. Journal of Geophysical Research 103, 3111 – 3118.

Ruessink, B. G., & Kroon, A. (1994). The behaviour of a multiple bar system in the nearshore zone of Terschelling, the Netherlands: 1965–1993. Marine Geology, 121(3), 187-197.

Shand, R. D. (2007). Bar splitting: system attributes and sediment budget implications for a net offshore migrating bar system. Journal of Coastal Research, (50): 721.

Short, A. D. (1985). Rip-current type, spacing and persistence, Narrabeen Beach, Australia. *Marine geology*, *65*(1-2), 47-71.

Short, A. D. (1991). Macro-meso tidal beach morphodynamics — an overview. Journal of Coastal Research 7, 417–436.

Short, A. D. & Hesp, P. A. (1982). Wave–beach–dune interaction in southeast Australia. Marine Geology 48, 259–84.

Simmonds, D. J., O'Hare, T. J., & Huntley, D. A. (1996). The influence of long waves on macrotidal beach morphology. Proceedings 25th International Conference on Coastal Engineering. ASCE, pp. 3090– 3103.

Sipka, V., & Anthony, E. J. (1999). Morphology and hydrodynamics of a macrotidal ridge and runnel beach under low wave conditions. Journal Recherche Oceanographique 24, 24– 31.

Sonu, C. J. (1973). Three-dimensional beach changes. The Journal of Geology, 81(1), 42-64.

Stepanian, A., & Levoy, F. (2003). Morphodynamical evolution sequences of intertidal bars on a macrotidal beach: case study of Omaha Beach (Normandy France). Oceanologica Acta 26, 167–177.

Stive, M. J. F., & De Vriend, H. J. (1994). Shear stresses and mean flow in shoaling and breaking waves. Proc. Int. Conf. Coastal Eng. ASCE, New York, pp. 594– 608.

Stockdon, H. F., Holman, R. A., & Sallenger, A. H. (2002). Parameterisation of incident and infragravity swash variance. Eos Trans. AGU, vol. 83 (47), p. F746. Fall Meet. Suppl.

Svendsen, I. A. (1984). Wave heights and set-up in a surf zone. Coastal Engineering 8(4), 303– 329.

Thom, B. G, & Hall, W. (1991). Behavior of beach profiles during accretion and erosion dominated periods. Earth Surface Processes and Landforms 16, 113–27.

Thornton, E. B., MacMahan, J., & Sallenger, A. H. (2007). Rip currents, mega-cusps, and eroding dunes. Marine geology, 240(1), 151-167.

Turner, I., Leyden, V., Symonds, G., McGrath, J., Jackson, A., Jancar, T., Aarninkhof, S. G. J., & Elshoff, I. E. (2001). Comparison of observed and predicted coastline changes at the gold coast artificial (surfing) reef, Sydney, Australia. *International Conference on Coastal Engineering*, Sydney, Australia.

Uunk, L. (2008). Automated collection of intertidal beach bathymetries from Argus video images (MSc Thesis). University of Twente/WL|Delft Hydraulics, 144p.

van de Lageweg, W. I., Bryan, K. R., Coco, G., & Ruessink, B. G. (2013). Observations of shoreline–sandbar coupling on an embayed beach. Marine Geology, 344, 101-114.

van der Weerd, L. (2012). Wave-driven dynamics of shoreward propagating accretionary waves in the nearshore (MSc Thesis). University of Twente/Deltares, 118p.

van Enckevort, I. M. J., & Ruessink, B. G. (2001). Effect of hydrodynamics and bathymetry on video estimates of nearshore sandbar position. *Journal of Geophysical Research: Oceans*, *106*(C8), 16969-16979.

van Enckevort, I. M. J., Ruessink, B. G., Coco, G., Suzuki., K., Turner, I. L., Plant, N. G., & Holman, R. A. (2004). Observations of nearshore crescentic sandbars. Journal of geophysical research, 109, C06028, doi:10.1029/2003JC002214.

van Houwelingen, S. T., Masselink, G., & Bullard, J. E. (2006). Characteristics and dynamics of multiple intertidal bars, North Lincolnshire, England. Earth Surface Processes and Landforms.

van Kuik, N. (2016) The effect of shoreface nourishments on Shoreward Propagating Accretionary Waves (Bachelor Thesis, University Utrecht).

van Rijn, L. C., Ruessink, B. G., & Mulder, J. P. M. (2002). Coast3DEgmond. The Behaviour of a Straight Sandy Coast on the Time Scale of Storms and Seasons. Aqua Publications, Amsterdam.

van Rijn, L. C., & Walstra, D. J. R. (2004). Analysis and modelling of shoreface nourishments. WL | Delft Hydraulics report Z3478.20.

Werner, B. T., & Fink, T. M. (1993). Beach cusps as self-organized patterns. Science, 260(5110), 968-972.

Wijnberg, K. M., & Holman, R. A. (2007). Video-observations of shoreward propagating accretionary waves. Proceedings of the RCEM 2007: 737-743.

Wijnberg, K. M., & Kroon, A. (2002). Barred beaches. Geomorphology, 48(1), 103-120.

Wijnberg, K. M., & Terwindt, J. H. (1995). Extracting decadal morphological behaviour from high-resolution, long-term bathymetric surveys along the Holland coast using eigenfunction analysis. Marine Geology, 126(1-4), 301-330.

Wright, L. D., Nielsen, P., Short, A. D., & Green, M. O. (1982). Morphodynamics of a macrotidal beach. Marine Geology 50, 97– 128.

Wright, L. D. & Short, A. D. (1984). Morphodynamic variability of surf zones and beaches: a synthesis. Marine Geology 56, 93–118.